



universität
wien

MASTERARBEIT / MASTER'S THESIS

Titel der Masterarbeit / Title of the Master's Thesis

„FINITE-DIFFERENCE MODELLING OF SEISMIC WAVES IN POROELASTIC MEDIUM“

verfasst von / submitted by

Dávid Gregor, Bc.

angestrebter akademischer Grad / in partial fulfilment of the requirements for the degree of
Master of Science (Msc)

Wien, 2016 / Vienna, 2016

Studienkennzahl lt. Studienblatt /
degree programme code as it appears on
the student record sheet:

A 066 680

Studienrichtung lt. Studienblatt /
degree programme as it appears on
the student record sheet:

Geophysics

Betreut von / Supervisor:

prof. RNDr. Peter Moczo, DrSc.

I hereby declare I wrote this thesis by myself, only with the help of referenced literature, under the careful supervision of my thesis supervisor.

Acknowledgment

First and foremost I wish to thank my advisor, professor Moczo, for his valuable advice, constructive criticism and insightful discussions and suggestions.

This thesis could not have been completed without the guidance and the help of associate professor Kristek who willingly devoted so much time in teaching me everything I know now about finite-difference method and computer programming.

I would like to thank my mom for her love, kindness and for always believing in me and encouraging me to follow my dreams. Her support from my first days of college to the capstone of a thesis has been both unquestioning and essential. I would also like to thank all my friends who supported me in writing.

Foreword

Seismology is one of the cornerstones of the modern Earth sciences that deals with the generation, propagation and recording of elastic waves in the Earth, which are both natural and human-made. Its major goal is to study earthquakes and the phenomena associated with them, such as propagation of elastic waves through the Earth. Seismic waves are the primary means by which scientists learn about Earth's deep interior, where direct observations are impossible. However, the main task of modern seismology is directly concerned with seeking ways to reduce their destructive impacts on humanity and predict their behavior at a site of interest.

In the last year of my Master's degree studies I was given a great opportunity to not only to continue my studies at Comenius University in Bratislava but also to become student of Vienna University and finish my major in Physics of the Earth at both universities. I do not regret this choice even though the study has become more difficult and more time-consuming than ever. I had a chance to hear the lectures from top scientist in their field of research, to learn from my peers and colleagues and to see the applications of geosciences not only in research but also in industry.

Throughout the last two years my passion for poroelasticity have not faded out despite of its complexity. Wave propagation in poroelastic material is of great importance in various diversified areas of science and engineering such as soil mechanics, seismology, acoustics, earthquake engineering and geophysics. In order to quantify effect of fluid-saturated porous media on ground motion, we need to consider poroelastic sedimentary structures. This complication introduced by complex structures leads to use of powerful computer to simulate ground motion more realistic, since analytical methods are precluded.

Content

Introduction	- 2 -
1 Numerical Modelling of Seismic-wave Propagation in Poroelastic Media: State-of-the-art	- 4 -
2 Objectives of the Master's Thesis	- 6 -
3 Equation of Motion and Constitutive Law	- 7 -
3.1 Equations for Elastic Medium	- 7 -
3.2 Equations for Poroelastic Medium	- 8 -
4 Finite-difference Modelling.....	- 11 -
4.1 Introduction	- 11 -
4.2 Computational domain and space-time grid.....	- 11 -
4.3 Velocity-stress FD scheme	- 12 -
4.4 Free surface.....	- 17 -
4.5 Perfectly matched layers.....	- 19 -
4.6 Source Implementation.....	- 22 -
5 Results	- 23 -
6 Conclusions.....	- 46 -
References	- 47 -

Introduction

Wave simulation is a theoretical field of research that began nearly three decades ago. Right from its early beginnings it has been in close relationship with the development of computer technology and numerical algorithms, which are mainly used for solving complex problems of mathematical analysis. In the field of computational physics, algorithms for solving problems using computers, represent useful tools that provide insight into wave propagation for variety of applications.

The primary application and the objective of this thesis is specially the wave simulation in poroelastic medium. Poroelastic theory is a useful model in many geological and even biological materials because almost all of these materials have an interstitial fluid in their pores. The fluid movement in rocks and soils has many features of importance to human populations and their settlements. Water supply, gas and oil removing belong to the most important. High water content can make soil masses unstable and previously stable slopes may fall over human developments. Another danger pose earthquakes that can cause fluid-saturated soil to liquefy and the building located upon them to sink into the soil mass. It is more than apparent from these examples that theory of poroelasticity requires our attention.

Dynamic porous media behavior is described by Biot's fundamental equations of poroelasticity. Biot's theory has been utilized for purposes of petroleum industry, in order to perform seismic surveys and determine the physical properties of rocks inside the reservoirs. Biot found that there are two dilatational waves and one rotational wave in a saturated porous medium. It has been observed that the dilatational wave of the second kind, also known as slow P-wave, is highly attenuated and is associated with a diffusion process. For this reason, the slow P-wave is significant only very close to the source or near material heterogeneities. However this only true for source frequencies that are much smaller than Biot's characteristic frequency ω_b , which strongly depends on friction of liquid inside the pores. As the source frequency increases or the friction is sufficiently decreased, the slow P-wave is activated. In process of simulation of wave propagation in poroelastic medium above the Biot's characteristic frequency the existence of viscous boundary layer at the pore walls must be taken into account. In this case the fluid flow is no longer laminar, the fluid velocity distribution within the pores is more complex, and the effects of viscosity are felt only in the thin boundary layer. The inertial effects are predominant and the slow wave becomes propagative. However, we have not allowed for the creation of viscous boundary layers in our modeling since the focus is strictly on the seismic band of frequencies.

At seismic frequencies, the mesoscopic loss mechanism seems to be the most important. For instance, mesoscopic-scale inhomogeneities (larger than the pore size but smaller than the

wavelength) such as mesoscopic patches of gas in a water-saturated sandstone are responsible of diffusion of pore fluid in and out between different patches, while dissipating energy through conversion of energy to the diffusive slow mode. Mesoscopic-losses are incorporated in White's model, which is based on approximations in the framework of Biot's theory.

In our master's thesis we only deal with the simplified model of poroelastic medium, namely isotropic homogeneous inviscid poroelastic half-space. We have applied numerical method, specifically finite-difference method to find approximated solution of poroelastic equations and to verify the method against the exact analytical solution.

The first chapter in our master's thesis is devoted to the current state-of-the-art in research and development of numerical techniques used for simulation of wave propagation in poroelastic materials. We briefly discuss the importance of modeling of the local Earth interior as two phase porous material, while referring to the different geometrical and rheological wavefield-porous-medium configurations elaborated by other authors.

In the second chapter we present objectives of this master's thesis.

The third chapter serves as an introduction to fundamental equations of poroelasticity-Biot's equations, summarizing equations of motion and constitutive equations, together with assumptions that were used during their derivation. The characteristic parameters of poroelastic materials are also presented here, but for more information, the reader is advised on author's bachelor thesis or on specific literature.

The primary goal of the fourth chapter is to provide basics of the finite-difference method and its application to the numerical modeling of seismic wave propagation in poroelastic media. We also make here detailed explanation of free surface condition, perfectly matched layers and line source implementation in case of 2D poroelastic wave simulation.

In the fifth chapter we present results. The chapter is followed by conclusions.

1 Numerical Modelling of Seismic-wave Propagation in Poroelastic Media: State-of-the-art

Numerical modeling of seismic wave propagation and earthquake motion in realistic media is an important tool used in seismology. During the past fifteen years, numerical simulation of wave propagation in fluid saturated poroelastic media has received more attention as its importance in geophysical exploration and reservoir characterization is now recognized, e.g., Carcione *et al.* (2010), Pride *et al.* (2004), Carcione *et al.* (2003). Although the soil can be approximated as a single phase elastic material, it is more accurate to treat soil as two phase composite material consisting of solid matrix and pore fluid. Moreover, many sedimentary and igneous rocks, and certain man-made materials (e.g., concrete) consist of solid framework surrounding a microscopic pore or fracture system saturated with fluids.

Few exact solutions to fundamental equations of poroelasticity exist, e.g., Dai *et al.* (1995), Burridge and Vargas (1979), Boutin *et al.* (1987), and are only for simplified media and source terms. Therefore, to apply poroelastic equations to more complex medium, numerical techniques must be used. Several different numerical techniques such as spectral-elements by Morency and Tromp (2008), pseudo-spectral methods by Carcione (1996), Özdenvar and McMechan (1997), discontinuous Galerkin method by de la Puente *et al.* (2008b) and finite-element method by Roberts and Garboczi (2002), can be used to solve these equations, but in this thesis, we solely focus on a finite-difference solution, which was studied by Zhu and McMechan (1991), Zhang (1999) and Dai *et al.* (1995). Numerous finite-difference techniques have been applied successfully to the wave equation in poroelastic medium. Staggered grids (SG), where variables and material properties are located at different positions on the grid cell, are the most common stable finite-difference scheme. The advantage of this scheme is to simulate wave propagation in heterogeneous media with a large variation in Poisson's ratio, which was shown by Moczo *et al.* (2000). Other modifications of finite-difference method, such as rotated staggered grid finite-difference method (RSG) by O'Brien (2010), exist. RSG can achieve higher accuracy for high medium contrasts and highly anisotropic media.

In earthquake ground motion research we are primary focused in near-surface local structures that in most cases must be modelled as a heterogeneous continuum. Sedimentary basins and valleys are examples of such a structures. Under specific circumstances we can approximate basin as a layer over homogeneous half-space. The model of poroelastic layer over poroelastic half-space was elaborated by various authors, e.g., Wang (2003), Dai *et al.* (1995) and Sheen *et al.* (2006). More complex formations were studied by Gurevich *et al.*

(1997), Shapiro and Muller (1999), Pride *et al.* (2002). As de la Cruz and Spanos (2001) have shown, the spatially varying porosity form another complex model, representing the earth poroelastic material more precisely.

As it was mentioned in introduction, the mesoscopic loss mechanism (wave-induced fluid flow) should be dominant at the seismic frequencies. White (1975) and White *et al.* (1975) demonstrate the mesoscopic-loss mechanism based on approximations of Biot's theory. They took into consideration the gas pockets in a water-saturated porous medium and the model of porous layers alternately saturated with water and gas. These models were called "patchy saturation" models. Dutta and Ode (1979) and Dutta and Seriff (1979) solved the problem exactly by using Biot's theory and confirmed the accuracy of White's results.

2 Objectives of the Master's Thesis

- algorithmization of mathematical formulation of equations of poroelasticity
- development of computational program
- testing of proposed algorithm and program

3 Equation of Motion and Constitutive Law

3.1 Equations for Elastic Medium

Seismology involves analysis of the ground motion produced by source within the Earth, such as for example earthquake faulting or explosion. Except in the immediate vicinity of the source, most of the ground motion is momentary, the ground returns to its initial position after the motion subsided. Vibrations of this type involve small elastic deformations, or strains, in response to internal forces in the rock, or stresses. The mathematical relationships between the stresses and strains in the material is embedded in the theory of elasticity. The theory of elasticity is elaborated by many authors such as for instance, Lay *et al.* (1995). Here we show only brief overview of theory of elasticity required for further use in the thesis.

Consider a perfectly elastic unbounded homogeneous continuum. The equation of motion (or elastodynamic equation) for such a medium has following form

$$\rho \ddot{u}_i = \sigma_{ij,j} + f_i \quad (3.1.1)$$

Let us restrict ourselves for an isotropic medium. Then the stress tensor is given by Hooke's law for the isotropic continuum denoted as

$$\sigma_{ij} = \lambda \delta_{ij} \varepsilon_{kk} + 2 \mu \varepsilon_{ij} \quad (3.1.2)$$

where λ and μ are Lamé elastic coefficients and ε_{ij} is the strain tensor

$$\varepsilon_{ij} = \frac{1}{2} (u_{i,j} + u_{j,i}) \quad (3.1.3)$$

Applying time derivative on equations (3.1.1)-(3.1.2) in the absence of source term f_i , one can obtain

$$\begin{aligned} \rho \dot{v}_i &= \dot{\sigma}_{ij,j} \\ \dot{\sigma}_{ij} &= \lambda \delta_{ij} \dot{\varepsilon}_{kk} + 2 \mu \dot{\varepsilon}_{ij} \end{aligned} \quad (3.1.4)$$

After substitution of time derivative of (3.1.3) into equation (3.1.4), we obtain

$$\begin{aligned} \rho \dot{v}_i &= \dot{\sigma}_{ij,j} \\ \dot{\sigma}_{ij} &= \lambda \delta_{ij} \dot{v}_{kk} + \mu (\dot{u}_{i,j} + \dot{u}_{j,i}) \end{aligned} \quad (3.1.5)$$

Equations (3.1.5) are written in the form of velocity \dot{v}_i and stress $\dot{\sigma}_{ij}$ and can be called the velocity-stress formulation of the equation of motion for the perfectly elastic, unbounded isotropic homogeneous continuum.

3.2 Equations for Poroelastic Medium

Equations of poroelastic medium (also known as Biot's equations) describe wave propagation in a porous saturated medium, i.e., a medium made of a solid frame (skeleton or matrix), fully saturated with a fluid, and accounts for the dissipation of energy due to the viscous pore fluid. Biot's theory arise from ignoring the microscopic level and assuming that continuum mechanics can be applied to measurable macroscopic quantities. He postulates the Lagrangian and uses Hamilton's principle to derive the equations governing wave propagation. The complete derivation of Biot's fundamental equations of poroelasticity can be found in our bachelor thesis or in pioneering work of Biot (1956).

In this work we consider a porous elastic body subjected to the following constraints:

- Displacements, strains and particle velocities are small. This allows to neglect the distinction between the Eulerian and Lagrangian formulations. The constitutive equations, dissipation forces, and kinetic momenta are linear.
- The wavelength is large in comparison with the dimensions of the pores. This is a requirement for applying the theory of continuum mechanics, and implies that scattering dissipation is neglected.
- The liquid phase is continuous, such that pores are connected and the disconnected pores are part of the matrix frame.
- Permeability and the material of the frame are isotropic and the medium is fully saturated.

We denote v_i as the velocity of the solid frame and V_i as the velocity of the fluid phase. Relative velocity q_i is defined as $\phi(V_i - v_i)$, where porosity ϕ is the volume fraction of the pore space. Using tensor notation and neglecting source terms, Biot's equations for an isotropic fluid-saturated porous medium are given by

$$\begin{aligned}\sigma_{ij,j} &= \rho \dot{v}_i + \rho_f \dot{q}_i \\ -p_{,i} &= \rho_f \dot{v}_i + m \dot{q}_i + b q_i\end{aligned}\tag{3.2.1}$$

Together with constitutive equations for total stress σ_{ij} and pore pressure p

$$\begin{aligned}\dot{\sigma}_{ij} &= \lambda \delta_{ij} v_{k,k} + \mu(v_{i,j} + v_{j,i}) - \alpha \dot{p} \delta_{ij} \\ \dot{p} &= -\alpha M v_{k,k} - M q_{k,k}\end{aligned}\tag{3.2.2}$$

form fundamental equations of poroelasticity.

The physical constants in equations describing the poroelastic medium along with some of their interdependencies are listed in Table 1.

Name	Units	Relation
ρ_f density of fluid phase	kg / m^3	_____
ρ_s density of solid phase	kg / m^3	_____
ϕ porosity	—	_____
ρ total density	kg / m^3	$(1 - \phi) \rho_s + \phi \rho_f$
η dynamic viscosity of fluid	$Pa s$	_____
κ permeability	m^2	_____
T tortuosity	—	_____
m mass coupling coefficient	kg / m^3	$\frac{T}{\phi} \rho_f$
b resistive damping(friction)	$Pa s / m^2$	$\frac{\eta}{\kappa}$
K_s bulk modulus of solid phase	Pa	_____
K_f bulk modulus of fluid phase	Pa	_____
K_d drained bulk modulus (bulk modulus of matrix)	Pa	_____
M Biot's modulus	Pa	$\frac{K_s}{1 - \phi - K_d / K_s + \phi K_s / K_f}$
α Biot-Willis stress coefficient	—	$1 - \frac{K_d}{K_s}$
μ shear modulus of solid phase	Pa	_____
λ_c undrained Lamé's coefficient	Pa	$K_d - \frac{2}{3} \mu + \alpha^2 M$

Table 1

Other interdependencies between parameters listed in Table 1 can be found in our bachelor thesis.

In order to study Biot's equations and constitutive equations using finite difference method, the equations must be rewritten in following velocity-stress (resp. velocity-stress-pressure) formulation

$$\begin{aligned}
(m\rho - \rho_f^2)\dot{v}_i &= m\sigma_{ij,j} + \rho_f b q_i + \rho_f p_{,i} \\
(m\rho - \rho_f^2)\dot{q}_i &= -\rho_f \sigma_{ij,j} - \rho b q_i - \rho p_{,i} \\
\dot{\sigma}_{ij} &= \mu(v_{i,j} + v_{j,i}) + \delta_{ij}(\lambda_c v_{k,k} + \alpha M q_{k,k}) \\
\dot{p} &= -\alpha M v_{k,k} - M q_{k,k}
\end{aligned} \tag{3.2.3}$$

For a 2-D case, the equations (3.2.3) can be expanded into following form

$$\begin{aligned}
\dot{v}_x &= \frac{1}{(m\rho - \rho_f^2)} \left(m\sigma_{xx,x} + m\sigma_{xz,z} + \rho_f b q_x + \rho_f p_{,x} \right) \\
\dot{v}_z &= \frac{1}{(m\rho - \rho_f^2)} \left(m\sigma_{xz,x} + m\sigma_{zz,z} + \rho_f b q_z + \rho_f p_{,z} \right) \\
\dot{q}_x &= -\frac{1}{(m\rho - \rho_f^2)} \left(\rho_f \sigma_{xx,x} + \rho_f \sigma_{xz,z} + \rho b q_x + \rho p_{,x} \right) \\
\dot{q}_z &= -\frac{1}{(m\rho - \rho_f^2)} \left(\rho_f \sigma_{xz,x} + \rho_f \sigma_{zz,z} + \rho b q_z + \rho p_{,z} \right) \\
\dot{\sigma}_{xx} &= (2\mu + \lambda_c) v_{x,x} + \lambda_c v_{z,z} + \alpha M q_{x,x} + \alpha M q_{z,z} \\
\dot{\sigma}_{xz} &= \mu (v_{x,z} + v_{z,x}) \\
\dot{\sigma}_{zz} &= \lambda_c v_{x,x} + (2\mu + \lambda_c) v_{z,z} + \alpha M q_{x,x} + \alpha M q_{z,z} \\
\dot{p} &= -\alpha M (v_{x,x} + v_{z,z}) - M (q_{x,x} + q_{z,z})
\end{aligned} \tag{3.2.4}$$

Last four equations in relation (3.2.4) can be expressed by means of time derivative of solid matrix strain tensor $\dot{\epsilon}_{ij}^m = \frac{1}{2} (\partial v_i / \partial x_j + \partial v_j / \partial x_i)$ and time derivative of variation of fluid content $\dot{\zeta} = -\partial_i q_i$ which then gives

$$\begin{aligned}
\dot{\sigma}_{xx} &= (2\mu + \lambda_c) \dot{\epsilon}_{xx}^m + \lambda_c \dot{\epsilon}_{zz}^m - \alpha M \dot{\zeta} \\
\dot{\sigma}_{xz} &= 2\mu \dot{\epsilon}_{xz}^m \\
\dot{\sigma}_{zz} &= \lambda_c \dot{\epsilon}_{xx}^m + (2\mu + \lambda_c) \dot{\epsilon}_{zz}^m - \alpha M \dot{\zeta} \\
\dot{p} &= -\alpha M (\dot{\epsilon}_{xx}^m + \dot{\epsilon}_{zz}^m) + M \dot{\zeta}
\end{aligned} \tag{3.2.5}$$

The formulation of equations of poroelasticity (3.2.5) is especially advantageous in case of PML incorporation, as we will see in subsequent chapter.

In order to distinguish the low-frequency regime from high-frequency regime we have to define Biot's characteristic frequency ω_B in the following form

$$\omega_B = 2\pi \frac{\eta \phi}{T K \rho_f} \tag{3.2.6}$$

In the present thesis, “high” and “low” frequencies will be referred to exclusively in terms of being above or below Biot's characteristic frequency (de la Puente *et al.* (2008a)). At low frequencies, the fluid flow in pores is laminar, on the other hand at high frequencies, the fluid flow is turbulent and change in this flow regime must be accommodated using frequency-dependent correction factor in the term involving resistive damping b . In the special case

when $\eta = 0$, resulting in zero value of b , the frequency regime is also considered to be “low”.

4 Finite-difference Modelling

4.1 Introduction

In this part we present a numerical method to solve Biot's equations in 2D homogeneous, fluid saturated poroelastic media based on a first order hyperbolic formulation whose unknowns consist of solid phase velocity, velocity of fluid phase relative to that of solid phase, solid stress, and fluid pressure.

We have developed algorithm for calculation of above-mentioned unknowns using finite-difference method as a common numerical technique for solving differential equations. In the finite-difference method variables and constants in the differential equation are discretized onto regular or irregular grid and the spatial and temporal derivatives are replaced by finite-difference operators acting on variables at specific locations. We have implemented this algorithm into computational program 2DFD_DVS, which is closely described in book Moczo *et al.* (2014). The employed finite-difference scheme has the properties of fourth order accuracy in space and second order in time. The corresponding scheme is said to be staggered, which means that different material properties and variables are defined at different locations on the grid. Moreover the scheme is explicit.

The method, we are adapting was elaborated by professor Moczo and associate professor Kristek in Moczo *et al.* (2000, 2002, 2004, 2007a, 2011, 2014), Kristek *et al.* (2002, 2009, 2010), Kristek and Moczo (2003), Moczo and Kristek (2005).

In following subchapters we will describe this method for 2D poroelastic wave propagation.

4.2 Computational domain and space-time grid

The most natural choice of the finite-difference grid for velocity-stress formulation is the staggered grid, in which each particle-velocity component and each shear stress-tensor component has its own grid position. The only exception is the same grid position for the diagonal stress-tensor components. Two-dimensional computational domain consists of rectangle in Cartesian coordinate system with the x -axis horizontal and positive to the right, and the y -axis negative downward. The horizontal top side of the rectangle represents planar free surface. Two vertical and one bottom side represent nonreflecting boundaries. Computational domain is covered by uniform space-time grid with grid spacing h .

4.3 Velocity-stress FD scheme

The eight coupled partial differential equations are numerically solved with an explicit, time-domain, FD method. Dependent variables are stored on uniformly-spaced, staggered, spatial grid. Figure 1 depicts the distribution of the variables over elementary rectangular cell of the 2D grid. Velocity components are stored on the top-right and bottom-left edges of the cell, while compressional stresses (resp. pressures) and shear stresses are on bottom-right and top-left edges, respectively. The corresponding poroelastic constants are also redistributed on elementary rectangular cell.

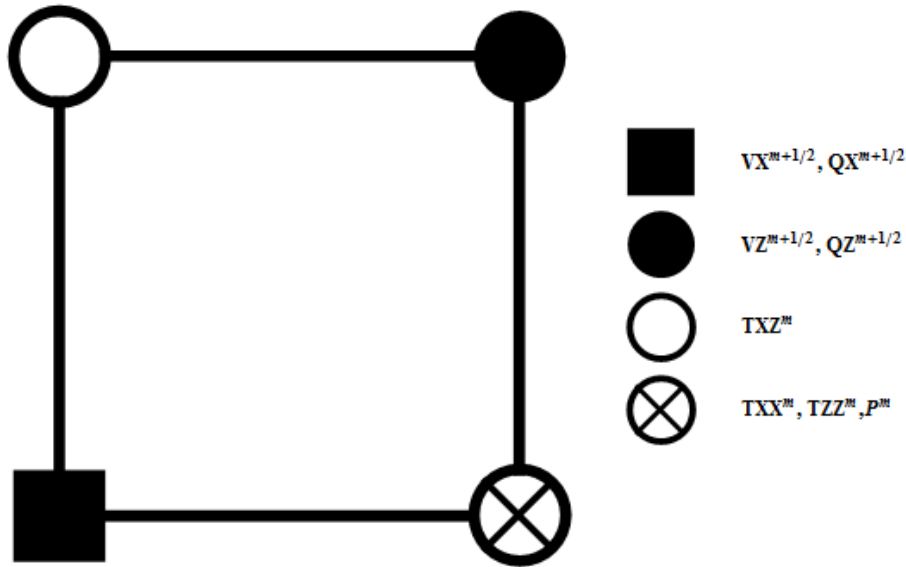


Figure 1 Grid cell of the staggered grid.

Using finite-difference method, equations (3.2.4) can be written in discretized form for FD method as

$$\begin{aligned}
VX_{I,L+1/2}^{m+1/2} &= VX_{I,L+1/2}^{m-1/2} + \\
&+ \frac{1}{(m\rho - \rho_f^2)_{I,L+1/2}} \frac{\Delta}{h} \left\{ m_{I,L+1/2} \left[\frac{9}{8} (TXX_{I+1/2,L+1/2}^m - TXX_{I-1/2,L+1/2}^m) \right. \right. \\
&- \frac{1}{24} (TXX_{I+3/2,L+1/2}^m - TXX_{I-3/2,L+1/2}^m) \\
&+ \left. \frac{9}{8} (TZX_{I,L+1}^m - TZX_{I,L}^m) - \frac{1}{24} (TZX_{I,L+2}^m - TZX_{I,L-1}^m) \right] \\
&+ (\rho_f b)_{I,L+1/2} \left[\frac{h}{2} (QX_{I,L+1/2}^{m+1/2} + QX_{I,L+1/2}^{m-1/2}) \right] \\
&+ \left. (\rho_f)_{I,L+1/2} \left[\frac{9}{8} (P_{I+1/2,L+1/2}^m - P_{I-1/2,L+1/2}^m) - \frac{1}{24} (P_{I+3/2,L+1/2}^m - P_{I-3/2,L+1/2}^m) \right] \right\} \quad (4.3.1)
\end{aligned}$$

$$\begin{aligned}
VZ_{I+1/2,L+1}^{m+1/2} &= VZ_{I+1/2,L+1}^{m-1/2} + \\
&+ \frac{1}{(m\rho - \rho_f^2)_{I+1/2,L+1}} \frac{\Delta}{h} \left\{ m_{I+1/2,L+1} \left[\frac{9}{8} (TXZ_{I+1,L+1}^m - TXZ_{I,L+1}^m) \right. \right. \\
&- \frac{1}{24} (TXZ_{I+2,L+1}^m - TXZ_{I-1,L+1}^m) \\
&+ \left. \frac{9}{8} (TZZ_{I+1/2,L+3/2}^m - TZZ_{I+1/2,L+1/2}^m) - \frac{1}{24} (TZZ_{I+1/2,L+5/2}^m - TZZ_{I+1/2,L-1/2}^m) \right] \\
&+ (\rho_f b)_{I+1/2,L+1} \left[\frac{h}{2} (QZ_{I+1/2,L+1}^{m+1/2} + QZ_{I+1/2,L+1}^{m-1/2}) \right] \\
&+ \left. (\rho_f)_{I+1/2,L+1} \left[\frac{9}{8} (P_{I+1/2,L+3/2}^m - P_{I+1/2,L+1/2}^m) - \frac{1}{24} (P_{I+1/2,L+5/2}^m - P_{I+1/2,L-1/2}^m) \right] \right\} \quad (4.3.2)
\end{aligned}$$

$$\begin{aligned}
QX_{I,L+1/2}^{m+1/2} &= \left(\frac{m\rho - \rho_f^2 - \frac{\rho b}{2} \Delta}{m\rho - \rho_f^2 + \frac{\rho b}{2} \Delta} \right)_{I,L+1/2} QX_{I,L+1/2}^{m-1/2} - \\
&- \frac{1}{\left(m\rho - \rho_f^2 + \frac{\rho b}{2} \Delta \right)_{I,L+1/2}} \frac{\Delta}{h} \left\{ (\rho_f)_{I,L+1/2} \left[\frac{9}{8} (TXX_{I+1/2,L+1/2}^m - TXX_{I-1/2,L+1/2}^m) \right. \right. \\
&- \frac{1}{24} (TXX_{I+3/2,L+1/2}^m - TXX_{I-3/2,L+1/2}^m) \\
&+ \left. \frac{9}{8} (TZX_{I,L+1}^m - TZX_{I,L}^m) - \frac{1}{24} (TZX_{I,L+2}^m - TZX_{I,L-1}^m) \right] \\
&+ \left. (\rho)_{I,L+1/2} \left[\frac{9}{8} (P_{I+1/2,L+1/2}^m - P_{I-1/2,L+1/2}^m) - \frac{1}{24} (P_{I+3/2,L+1/2}^m - P_{I-3/2,L+1/2}^m) \right] \right\} \quad (4.3.3)
\end{aligned}$$

$$\begin{aligned}
QZ_{I+1/2,L+1}^{m+1/2} &= \left(\frac{m\rho - \rho_f^2 - \frac{\rho b}{2}\Delta}{m\rho - \rho_f^2 + \frac{\rho b}{2}\Delta} \right)_{I,L+1/2} QZ_{I+1/2,L+1}^{m-1/2} - \\
&- \frac{1}{\left(m\rho - \rho_f^2 + \frac{\rho b}{2}\Delta \right)_{I+1/2,L+1}} \frac{\Delta}{h} \left\{ (\rho_f)_{I+1/2,L+1} \left[\frac{9}{8} (TXZ_{I+1,L+1}^m - TXZ_{I,L+1}^m) \right. \right. \\
&- \frac{1}{24} (TXZ_{I+2,L+1}^m - TXZ_{I-1,L+1}^m) \\
&+ \left. \frac{9}{8} (TZZ_{I+1/2,L+3/2}^m - TZZ_{I+1/2,L+1/2}^m) - \frac{1}{24} (TZZ_{I+1/2,L+5/2}^m - TZZ_{I+1/2,L-1/2}^m) \right] \\
&+ \left. (\rho)_{I+1/2,L+1} \left[\frac{9}{8} (P_{I+1/2,L+3/2}^m - P_{I+1/2,L+1/2}^m) - \frac{1}{24} (P_{I+1/2,L+5/2}^m - P_{I+1/2,L-1/2}^m) \right] \right\}
\end{aligned} \tag{4.3.4}$$

$$\begin{aligned}
TXX_{I+1/2,L+1/2}^m &= TXX_{I+1/2,L+1/2}^{m-1} \\
&+ \frac{\Delta}{h} \{ (\lambda_c + 2\mu)_{I+1/2,L+1/2} \left[\frac{9}{8} (VX_{I+1,L+1/2}^{m-1/2} - VX_{I,L+1/2}^{m-1/2}) - \frac{1}{24} (VX_{I+2,L+1/2}^{m-1/2} - VX_{I-1,L+1/2}^{m-1/2}) \right] \right. \\
&+ (\lambda_c)_{I+1/2,L+1/2} \left[\frac{9}{8} (VZ_{I+1/2,L+1}^{m-1/2} - VZ_{I+1/2,L}^{m-1/2}) - \frac{1}{24} (VZ_{I+1/2,L+2}^{m-1/2} - VZ_{I+1/2,L-1}^{m-1/2}) \right] \\
&+ (\alpha M)_{I+1/2,L+1/2} \left[\frac{9}{8} (QX_{I+1,L+1/2}^{m-1/2} - QX_{I,L+1/2}^{m-1/2}) - \frac{1}{24} (QX_{I+2,L+1/2}^{m-1/2} - QX_{I-1,L+1/2}^{m-1/2}) \right] \\
&+ \left. (\alpha M)_{I+1/2,L+1/2} \left[\frac{9}{8} (QZ_{I+1/2,L+1}^{m-1/2} - QZ_{I+1/2,L}^{m-1/2}) - \frac{1}{24} (QZ_{I+1/2,L+2}^{m-1/2} - QZ_{I+1/2,L-1}^{m-1/2}) \right] \right\}
\end{aligned} \tag{4.3.5}$$

$$\begin{aligned}
TXZ_{I,L+1}^m &= TXZ_{I,L+1}^{m-1} \\
&+ \frac{\Delta}{h} \left\{ \mu_{I,L+1} \left[\frac{9}{8} (VX_{I,L+3/2}^{m-1/2} - VX_{I,L+1/2}^{m-1/2}) - \frac{1}{24} (VX_{I,L+5/2}^{m-1/2} - VX_{I,L-1/2}^{m-1/2}) \right] \right. \\
&+ \left. \mu_{I,L+1} \left[\frac{9}{8} (VZ_{I+1/2,L+1}^{m-1/2} - VZ_{I-1/2,L+1}^{m-1/2}) - \frac{1}{24} (VZ_{I+3/2,L+1}^{m-1/2} - VZ_{I-3/2,L+1}^{m-1/2}) \right] \right\}
\end{aligned} \tag{4.3.6}$$

$$\begin{aligned}
TZZ_{I+1/2,L+1/2}^m &= TZZ_{I+1/2,L+1/2}^{m-1} \\
&+ \frac{\Delta}{h} \{(\lambda_c)_{I+1/2,L+1/2} \left[\frac{9}{8} (VX_{I+1,L+1/2}^{m-1/2} - VX_{I,L+1/2}^{m-1/2}) - \frac{1}{24} (VX_{I+2,L+1/2}^{m-1/2} - VX_{I-1,L+1/2}^{m-1/2}) \right] \right. \\
&+ (\lambda_c + 2\mu)_{I+1/2,L+1/2} \left[\frac{9}{8} (VZ_{I+1/2,L+1}^{m-1/2} - VZ_{I+1/2,L}^{m-1/2}) - \frac{1}{24} (VZ_{I+1/2,L+2}^{m-1/2} - VZ_{I+1/2,L-1}^{m-1/2}) \right] \\
&+ (\alpha M)_{I+1/2,L+1/2} \left[\frac{9}{8} (QX_{I+1,L+1/2}^{m-1/2} - QX_{I,L+1/2}^{m-1/2}) - \frac{1}{24} (QX_{I+2,L+1/2}^{m-1/2} - QX_{I-1,L+1/2}^{m-1/2}) \right] \\
&+ (\alpha M)_{I+1/2,L+1/2} \left[\frac{9}{8} (QZ_{I+1/2,L+1}^{m-1/2} - QZ_{I+1/2,L}^{m-1/2}) - \frac{1}{24} (QZ_{I+1/2,L+2}^{m-1/2} - QZ_{I+1/2,L-1}^{m-1/2}) \right]
\end{aligned} \quad (4.3.7)$$

$$\begin{aligned}
P_{I+1/2,L+1/2}^m &= P_{I+1/2,L+1/2}^{m-1} \\
&- \frac{\Delta}{h} \{(\alpha M)_{I+1/2,L+1/2} \left[\frac{9}{8} (VX_{I+1,L+1/2}^{m-1/2} - VX_{I,L+1/2}^{m-1/2}) - \frac{1}{24} (VX_{I+2,L+1/2}^{m-1/2} - VX_{I-1,L+1/2}^{m-1/2}) \right] \right. \\
&+ (\alpha M)_{I+1/2,L+1/2} \left[\frac{9}{8} (VZ_{I+1/2,L+1}^{m-1/2} - VZ_{I+1/2,L}^{m-1/2}) - \frac{1}{24} (VZ_{I+1/2,L+2}^{m-1/2} - VZ_{I+1/2,L-1}^{m-1/2}) \right] \\
&+ (M)_{I+1/2,L+1/2} \left[\frac{9}{8} (QX_{I+1,L+1/2}^{m-1/2} - QX_{I,L+1/2}^{m-1/2}) - \frac{1}{24} (QX_{I+2,L+1/2}^{m-1/2} - QX_{I-1,L+1/2}^{m-1/2}) \right] \\
&+ (M)_{I+1/2,L+1/2} \left[\frac{9}{8} (QZ_{I+1/2,L+1}^{m-1/2} - QZ_{I+1/2,L}^{m-1/2}) - \frac{1}{24} (QZ_{I+1/2,L+2}^{m-1/2} - QZ_{I+1/2,L-1}^{m-1/2}) \right]
\end{aligned} \quad (4.3.8)$$

Symbols Δ and h represent time step and grid spacing, respectively. In equation (4.3.1)-(4.3.8) we approximate velocity q_x and q_z by time average in following manner

$$\begin{aligned}
q_x|_{I,L}^m &\approx \frac{1}{2} (QX_{I+1/2,L+1}^{m+1/2} + QX_{I+1/2,L+1}^{m-1/2}) \\
q_z|_{I,L}^m &\approx \frac{1}{2} (QZ_{I+1/2,L+1}^{m+1/2} + QZ_{I+1/2,L+1}^{m-1/2})
\end{aligned} \quad (4.3.9)$$

The equations (4.3.1)-(4.3.8) can be further simplified using following substitution for poroelastic constants

$$\begin{aligned}
A_x &= \left(\frac{m}{m\rho - \rho_f^2} \right)_{I,L+1/2} & A_z &= \left(\frac{m}{m\rho - \rho_f^2} \right)_{I+1/2,L+1} \\
B_x &= \left(\frac{\rho_f b}{m\rho - \rho_f^2} \right)_{I,L+1/2} & B_z &= \left(\frac{\rho_f b}{m\rho - \rho_f^2} \right)_{I+1/2,L+1} \\
C_x &= \left(\frac{\rho_f}{m\rho - \rho_f^2} \right)_{I,L+1/2} & C_z &= \left(\frac{\rho_f}{m\rho - \rho_f^2} \right)_{I+1/2,L+1} \\
D_x &= \left(\frac{m\rho - \rho_f^2 - \frac{\rho b}{2}\Delta}{m\rho - \rho_f^2 + \frac{\rho b}{2}\Delta} \right)_{I,L+1/2} & D_z &= \left(\frac{m\rho - \rho_f^2 - \frac{\rho b}{2}\Delta}{m\rho - \rho_f^2 + \frac{\rho b}{2}\Delta} \right)_{I+1/2,L+1} \\
E_x &= \left(\frac{\rho_f}{m\rho - \rho_f^2 + \frac{\rho b}{2}\Delta} \right)_{I,L+1/2} & E_z &= \left(\frac{\rho_f}{m\rho - \rho_f^2 + \frac{\rho b}{2}\Delta} \right)_{I+1/2,L+1} \\
F_x &= \left(\frac{\rho}{m\rho - \rho_f^2 + \frac{\rho b}{2}\Delta} \right)_{I,L+1/2} & F_z &= \left(\frac{\rho}{m\rho - \rho_f^2 + \frac{\rho b}{2}\Delta} \right)_{I+1/2,L+1}
\end{aligned} \tag{4.3.10}$$

Note that all constants from A_x to F_z in equations (4.3.10) have same unit as one over density, that is $kg^{-1} m^3$. This is advantageous in case of simulating wave propagation in multiple layer system with material discontinuities. Moczo *et al.* (2002) proposed finite-difference scheme based on a heterogeneous formulation of equation of motion for modeling seismic wave propagation in elastic media. They explicitly constructed heterogeneous displacement-stress finite-difference scheme with the volume harmonic averaging of the shear modulus and the bulk modulus, and volume arithmetic averaging of the density which is based on simplified boundary conditions inside heterogeneous media and which allows for arbitrary position of the material discontinuity in the spatial grid. This approach could be used also for poroelastic media.

4.4 Free surface

The free surface boundary condition aims at representing the contact of poroelastic material with vacuum. At this boundary, both the stresses and fluid pressure vanish. If surface S is planar and perpendicular to the z -axis, this implies

$$\sigma_{iz} = 0, \quad p = 0; \quad i \in \{x, z\} \quad (4.4.1)$$

After following restrictions (4.4.1) last three equations (3.2.4) become

$$\begin{aligned} (2\mu + \lambda_c) \frac{\partial v_z}{\partial z} + \lambda_c \frac{\partial v_x}{\partial x} + \alpha M \left(\frac{\partial q_x}{\partial x} + \frac{\partial q_z}{\partial z} \right) &= 0 \\ \frac{\partial v_z}{\partial x} + \frac{\partial v_x}{\partial z} &= 0 \\ \alpha \frac{\partial v_z}{\partial x} + \frac{\partial v_x}{\partial z} + \left(\frac{\partial q_x}{\partial x} + \frac{\partial q_z}{\partial z} \right) &= 0 \\ \left(\frac{\partial q_x}{\partial x} + \frac{\partial q_z}{\partial z} \right) &= 0 \end{aligned} \quad (4.4.2)$$

Note that the last relation in (4.4.2) does not follow from restriction (4.4.1). This last equation of equations (4.4.2) is due to the fact that on the free surface, shear stress vanishes for both the solid and the fluid phases. Thus we have four equations to solve for four unknowns v_x, v_z, q_x and q_z .

In order to simulate planar free surface in the 2D 4th-order staggered-grid finite-difference scheme, we use stress-imaging technique proposed by Levander (1988). Other methods might be used, such as adjusted finite-difference approximation developed by Kristek *et al.* (2002) and Moczo *et al.* (2004).

Stress imaging in the (2,4) VS SG scheme

In the staggered grid there are two options for localizing the planar free surface. In the first approach, the free surface is placed at the horizontal grid plane going through the positions of the horizontal velocity components v_x, q_x , stress-tensor components σ_{xx}, σ_{zz} and fluid pressure p . We indicate this formulation by letter H. In the second approach, the planar free surface coincides with the horizontal grid plane going through the positions of v_z, q_z, σ_{zx} . We indicate this formulation by letter W. In our program we use only W formulation of stress imaging. Therefore, we present here only this formulation.

The W formulation: The position of the free surface and quantities above the free surface is shown in Figure 2. The formulation can be summarized as follows:

$$TZX(0) = 0$$

$$TZZ(-h/2) = -TZZ(h/2)$$

$$P(-h/2) = -P(h/2)$$

$$TZX(-h) = -TZX(h)$$

$$TZZ(-3h/2) = -TZZ(3h/2)$$

$$P(-3h/2) = -P(3h/2)$$

$VZ(0)$ and $QZ(0)$ are obtained from 4th-order approximation to the equation of motion in

which $\frac{\partial \sigma_{zz}}{\partial z}$ is obtained also using imaged σ_{zz} values.

$VX(-h/2)$ is obtained from 4th-order approximation of the second equation of (4.4.2)

$QX(-h/2)$ is obtained from 4th-order approximation of the fourth equation of (4.4.2)

$VZ(-h)$ and $QZ(-h)$ are obtained from 4th-order approximation of the first and third equations of (4.4.2)

Other quantities are treated according to scheme (4.3.1)-(4.3.8).

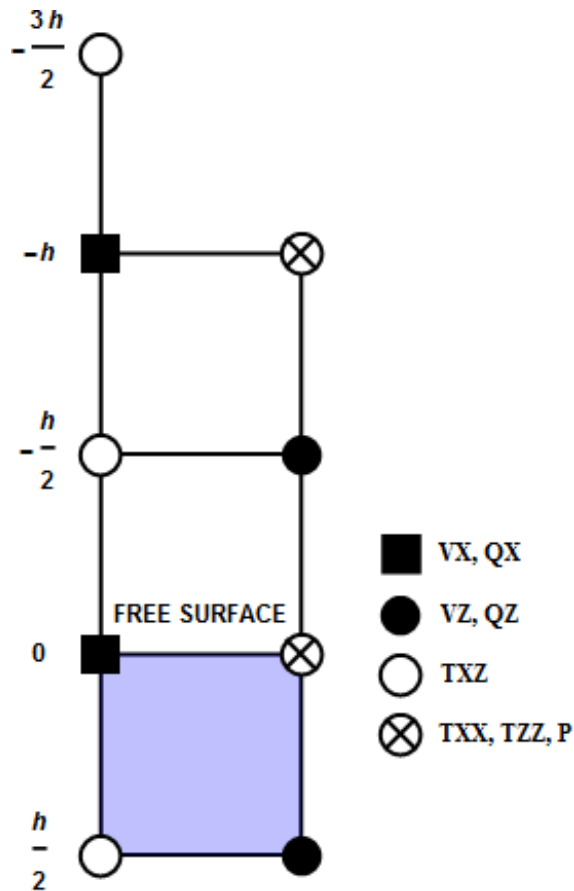


Figure 2 Grid cells in vicinity of free surface.

4.5 Perfectly matched layers

In this chapter we are primary following work of Kristek *et al.* (2009) and Komatitsch and Martin (2008). The perfectly matched layers are used at the computational edge to absorb the outgoing waves. Here we present unsplit formulation of PML.

We replace spatial differentiation operator $\partial/\partial x_i$ in equations (3.2.3) by the differentiation operator

$$\frac{\partial}{\partial \tilde{x}_i} = \frac{1}{s} \frac{\partial}{\partial x_i} \quad (4.5.1)$$

where s is stretching factor

$$s = \gamma + \frac{\Omega}{\alpha + i\omega} \quad (4.5.2)$$

and γ, Ω and α being, in general, function of x_i .

For special case with $\gamma = 1$ and $\alpha = 0$ equation (4.5.2) yields

$$s = 1 + \frac{\Omega}{i\omega} \quad (4.5.3)$$

In our simations we have considered this very case above.

Using expression (4.5.2), equations (3.2.3) together with relations for solid matrix strain and fluid content variation defined in Chapter 3.2 can be modified using Fourier transform into this particular form

$$\begin{aligned} i\omega(m\rho - \rho_f^2)v_i &= m\frac{1}{s}\sigma_{i,j,j} + \rho_f b q_i + \rho_f \frac{1}{s}p_{,i} \\ i\omega(m\rho - \rho_f^2)q_i &= -\rho_f \frac{1}{s}\sigma_{i,j,j} - \rho b q_i - \rho \frac{1}{s}p_{,i} \\ i\omega\sigma_{ij} &= \mu\frac{1}{s}(v_{i,j} + v_{j,i}) + \delta_{ij}\frac{1}{s}(\lambda_c v_{k,k} + \alpha M q_{k,k}) \\ i\omega p &= -\alpha M \frac{1}{s}v_{k,k} - M \frac{1}{s}q_{k,k} \\ i\omega\epsilon_{ij}^m &= \frac{1}{2s}(v_{i,j} + v_{j,i}) \\ i\omega\zeta &= -\frac{1}{s}q_{k,k} \end{aligned} \quad (4.5.4)$$

In order to simplify the PML equations, the field variables are split as follows

$$\begin{aligned}
v_i &= v_i^1 + v_i^2 \\
q_i &= q_i^1 + q_i^2 \\
\varepsilon_{ij} &= \varepsilon_{ij}^1 + \varepsilon_{ij}^2 \\
\varsigma &= \varsigma^1 + \varsigma^2
\end{aligned} \tag{4.5.5}$$

Equations (4.5.4), using (4.5.5), can be according to Zeng and Liu (2001 b) written as

$$\begin{aligned}
i\omega(m\rho - \rho_f^2)v_x^x &= \frac{1}{s}m\sigma_{xx,x} + \frac{1}{s}\rho_f p_{,x} + m\sigma_{xz,z} \\
i\omega(m\rho - \rho_f^2)v_x^y &= \frac{1}{s}m\sigma_{xy,y} + m\sigma_{xx,x} + \rho_f b q_x \\
i\omega(m\rho - \rho_f^2)v_y^x &= \frac{1}{s}m\sigma_{xy,x} + m\sigma_{zz,z} \\
i\omega(m\rho - \rho_f^2)v_y^y &= \frac{1}{s}m\sigma_{yy,y} + \frac{1}{s}\rho_f p_{,y} + m\sigma_{xz,x} + \rho_f b q_y \\
i\omega(m\rho - \rho_f^2)q_x^x &= -\frac{1}{s}\rho_f \sigma_{xx,x} - \frac{1}{s}\rho p_{,x} - \rho_f \sigma_{xz,z} \\
i\omega(m\rho - \rho_f^2)q_x^y &= -\frac{1}{s}\rho_f \sigma_{xy,y} - \rho_f \sigma_{xx,x} - \rho b q_x \\
i\omega(m\rho - \rho_f^2)q_y^x &= -\frac{1}{s}\rho_f \sigma_{xy,x} - \rho_f \sigma_{zz,z} \\
i\omega(m\rho - \rho_f^2)q_y^y &= -\frac{1}{s}\rho_f \sigma_{yy,y} - \frac{1}{s}\rho p_{,y} - \rho_f \sigma_{xz,x} - \rho b q_y \\
i\omega\varepsilon_{xy}^x &= \frac{1}{2s}v_{y,x} \\
i\omega\varepsilon_{xy}^y &= \frac{1}{2s}v_{x,y} \\
i\omega\varepsilon_{ii} &= \frac{1}{s}v_{i,i} \\
i\omega\varsigma^x &= -\frac{1}{s}q_{x,x} \\
i\omega\varsigma^y &= -\frac{1}{s}q_{y,y}
\end{aligned} \tag{4.5.6}$$

By rewriting $1/s$ in following form

$$\frac{1}{\gamma} - \frac{b}{a + i\omega} \tag{4.5.7}$$

where

$$a = -\alpha + \frac{\Omega}{\gamma}, \quad b = \frac{\Omega}{\gamma^2} \tag{4.5.8}$$

and defining memory variables $\theta_j^i, \psi_i^j, \vartheta_j^i, \phi_i^j, \zeta_j^i, \xi_i^j$ for $i = x, z; j = x, z$; satisfying following ordinary differential equations

$$\begin{aligned}
\dot{\theta}_x^x + a\theta_x^x &= -b\sigma_{xx,x}, \quad \dot{\psi}_x^x + a\psi_x^x = -b p_{,x} & \dot{\vartheta}_x^x + a\vartheta_x^x &= -b\sigma_{xx,x}, \quad \dot{\phi}_x^x + a\phi_x^x = -b p_{,x} \\
\dot{\theta}_x^z + a\theta_x^z &= -b\sigma_{xz,z} & \dot{\vartheta}_x^z + a\vartheta_x^z &= -b\sigma_{xz,z} \\
\dot{\theta}_z^x + a\theta_z^x &= -b\sigma_{xz,x} & \dot{\vartheta}_z^x + a\vartheta_z^x &= -b\sigma_{xz,x} \\
\dot{\theta}_z^z + a\theta_z^z &= -b\sigma_{zz,z}, \quad \dot{\psi}_z^z + a\psi_z^z = -b p_{,z} & \dot{\vartheta}_z^z + a\vartheta_z^z &= -b\sigma_{zz,z}, \quad \dot{\phi}_z^z + a\phi_z^z = -b p_{,z}
\end{aligned}$$

$$\begin{aligned}
\dot{\zeta}_z^x + a\zeta_z^x &= -\frac{b}{2}v_{z,x} & \dot{\xi}_x^x + a\xi_z^z &= -b q_{x,x} \\
\dot{\zeta}_x^z + a\zeta_x^z &= -\frac{b}{2}v_{x,z} & \dot{\xi}_z^z + a\xi_z^z &= -b q_{z,z} \\
\dot{\zeta}_x^x + a\zeta_x^x &= -b v_{x,x} \\
\dot{\zeta}_z^z + a\zeta_z^z &= -b v_{z,z}
\end{aligned}$$

(4.5.9)

one can obtain ,after applying Inverse Fourier Transform, the modification of equations (4.5.6) in following form

$$\begin{aligned}
(m\rho - \rho_f^2)v_x^x &= \frac{1}{\gamma}m\sigma_{xx,x} + m\theta_x^x + \frac{1}{\gamma}\rho_f p_{,x} + \rho_f\psi_x^x + m\sigma_{xz,z} \\
(m\rho - \rho_f^2)v_x^z &= \frac{1}{\gamma}m\sigma_{xz,z} + m\theta_x^z + m\sigma_{xx,x} + \rho_f b q_x \\
(m\rho - \rho_f^2)v_z^x &= \frac{1}{\gamma}m\sigma_{xz,x} + m\theta_z^x + m\sigma_{zz,z} \\
(m\rho - \rho_f^2)v_z^z &= \frac{1}{\gamma}m\sigma_{zz,z} + m\theta_z^z + \frac{1}{\gamma}\rho_f p_{,z} + \rho_f\psi_z^z + m\sigma_{xz,x} + \rho_f b q_z \\
(m\rho - \rho_f^2)q_x^x &= -\frac{1}{\gamma}\rho_f\sigma_{xx,x} - \rho_f\vartheta_x^x - \frac{1}{\gamma}\rho p_{,x} - \rho\phi_x^x - \rho_f\sigma_{xz,z} \\
(m\rho - \rho_f^2)q_x^z &= -\frac{1}{\gamma}\rho_f\sigma_{xz,z} - \rho_f\vartheta_x^z - \rho_f\sigma_{xx,x} - \rho b q_x \\
(m\rho - \rho_f^2)q_z^x &= -\frac{1}{\gamma}\rho_f\sigma_{xz,x} - \rho_f\vartheta_z^x - \rho_f\sigma_{zz,z} \\
(m\rho - \rho_f^2)q_z^z &= -\frac{1}{\gamma}\rho_f\sigma_{zz,z} - \rho_f\vartheta_z^z - \frac{1}{\gamma}\rho p_{,z} - \rho\phi_z^z - \rho_f\sigma_{xz,x} - \rho b q_z
\end{aligned} \tag{4.5.10}$$

$$\begin{aligned}
\dot{\epsilon}_{xz}^x &= \frac{1}{2\gamma} v_{z,x} + \zeta_z^x \\
\dot{\epsilon}_{xz}^z &= \frac{1}{2\gamma} v_{x,z} + \zeta_x^z \\
\dot{\epsilon}_{ii} &= \frac{1}{\gamma} v_{i,i} + \zeta_i^i \\
\dot{\zeta}^x &= -\frac{1}{\gamma} q_{x,x} - \xi_x^x \\
\dot{\zeta}^z &= -\frac{1}{\gamma} q_{z,z} - \xi_z^z
\end{aligned}$$

Equations (4.5.10) represent final form of PML formulation of poroelastic equations.

4.6 Source Implementation

The poroelastic formulation involves two distinct phases present within a porous medium, while forces might be applied on both of them. A body-force source acting on the solid frame is available as well as pressure sources acting on the bulk material, the pore fluid, or a combination of both. Generally, the application of the source considers four cases.

In the first case is energy partitioned between the two phases by multiplying fluid phase source-time function s_f and solid phase source-time function s_s with factor ϑ . Then the resulting source terms f_s and f_f acquire following form

$$f_s(t) = (1 - \vartheta)s_s(t), \quad f_f(t) = \vartheta s_s(t) \quad (4.6.1)$$

where ϑ is usually equal to porosity ϕ .

Second case and third case of source partitioning consist in applying force purely on solid phase, while ϑ in equations (4.6.1) is equal to zero or in applying force purely on fluid, while setting ϑ in the same equations to one, respectively.

In the last case, the force is applied to both the solid and the fluid phase with the same amplitude (one), so both factors $(1 - \vartheta)$ and ϑ are equal to one.

In this thesis we solely used as source-time function the Gaussian function

$$s(t) = \frac{1}{2\pi^2 f_0^2} e^{-(\pi f_0(t - t_0))^2} \quad (4.6.2)$$

where t_0 is the time delay and f_0 is the dominant frequency. Source terms can be added to equations (3.2.3) depending on the specific source implementation that is to be simulated. In our tests we have considered explosive line source as a stress increment for both the diagonal stresses and pore pressure.

5 Results

In this section we demonstrate our results for a line source in an unbounded homogeneous poroelastic medium. As we have stated in Chapter 4.4, the free surface condition is implemented in our computational program, but for purpose of numerical solution against analytical, we have situated source and receivers in such depth and taken such time window that reflected waves from free surface are not present on synthetic seismograms. Therefore for this special case, we can consider our model as an unbounded poroelastic medium.

As we have already mentioned earlier, the existence of a slow compressional wave is indication that the medium is a porous. Therefore the homogeneous poroelastic half-space is not only defined by the P-wave speed VP_f and S-wave speed VS , but also by the slow P-wave speed VP_s . Values of wave speeds can be calculated theoretically (Carcione 1996b). Values of wave speeds together with material parameters introduced in Chapter 3.2 are listed in Table 2.

Material parameters	
$VP_f \left(m \, s^{-1} \right)$	2639
$VP_s \left(m \, s^{-1} \right)$	960
$VS \left(m \, s^{-1} \right)$	1449
$\rho_s \left(kg \, m^{-3} \right)$	2650
$\rho_f \left(kg \, m^{-3} \right)$	880
$\rho \left(kg \, m^{-3} \right)$	2473
$K_s \left(GPa \right)$	12.2
$K_f \left(GPa \right)$	1.985
$K_d \left(GPa \right)$	9.6
$\mu \left(GPa \right)$	5.1
ϕ	0.1
$\eta \left(Pa \, s \right)$	0

	Model 1	Model 2	Model 3
Source parameters			
$f_{\min} \left(Hz \right)$		0.2	
$f_{\max} \left(Hz \right)$		120	
$f_0 \left(Hz \right)$		30	
$t_0 \left(s \right)$		0.04	
Parameters of numerical simulation			
$\Delta t \left(s \right)$		$0.1 \, \Delta t_{\max}$	
$h \left(m \right)$	5	3	1.5
$\lambda_{\max} \left(m \right)$		13195	
$\lambda_{\min} \left(m \right)$		8	

Table 3			
---------	--	--	--

Table 2

Table 3

The wavefield is generated by an explosive dilatational line source partitioned between two phases according to the forth case, mentioned in Source Implementation Chapter. Its time function is given by Gaussian function $s(t) = e^{-(\pi f_0(t - t_0))^2} / 2 \pi^2 f_0^2$ with dominant frequency f_0 and time shift t_0 listed in Table 3.

Source-time function is pictured in Figure 3, together with its spectrum.

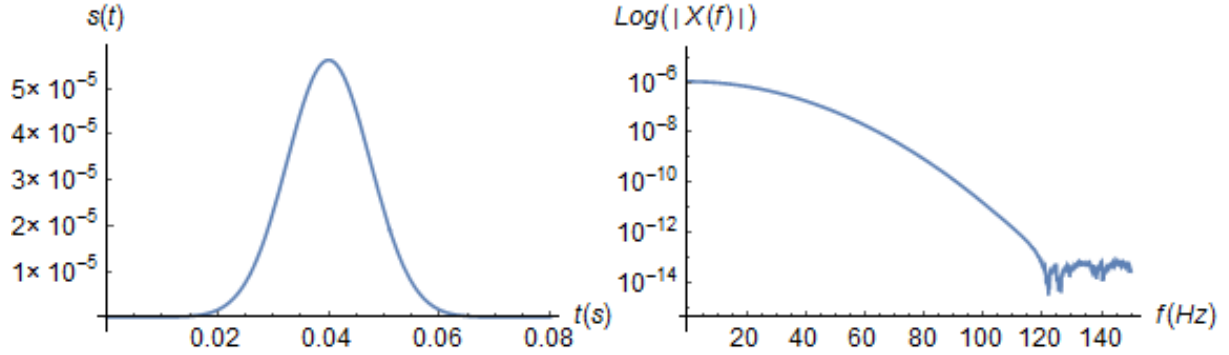


Figure 3 Source-time function.

The simulations are performed in frequency band from 0.2 Hz up to 80 Hz. The upper bound of frequency band corresponds to decrease of spectral amplitude by approximately three orders.

For simulation purposes, we have considered 3 models, while each of them has different value of grid spacing. The different grid spacing values were picked, in order to demonstrate accuracy of solution and undesirable grid dispersion. The parameters of numerical simulations for different Models are listed in Table 3.

The expression for maximal time step Δt_{\max} for two-dimensional case was derived by following work of O'Brien (2010). The following relation represents maximal time step

$$\Delta t_{\max} = \frac{h}{\sqrt{2}} \frac{6}{7} \sqrt{\frac{s_2 - \sqrt{s_2^2 - 4 s_1 s_3}}{s_3}} \quad (5.1.1)$$

where

$$\begin{aligned} s_1 &= m \rho - \rho_f^2 \\ s_2 &= m(\lambda_c + 2\mu) + \rho M - 2\alpha M \rho_f \\ s_3 &= M \lambda_c + 2\mu M - \alpha^2 M^2 \end{aligned} \quad (5.1.2)$$

The source-receiver configuration is depicted in Figure 4 with positive x -axis going from left to right and negative z -axis going from up to down, while the origin of coordinate system is in left-top corner.

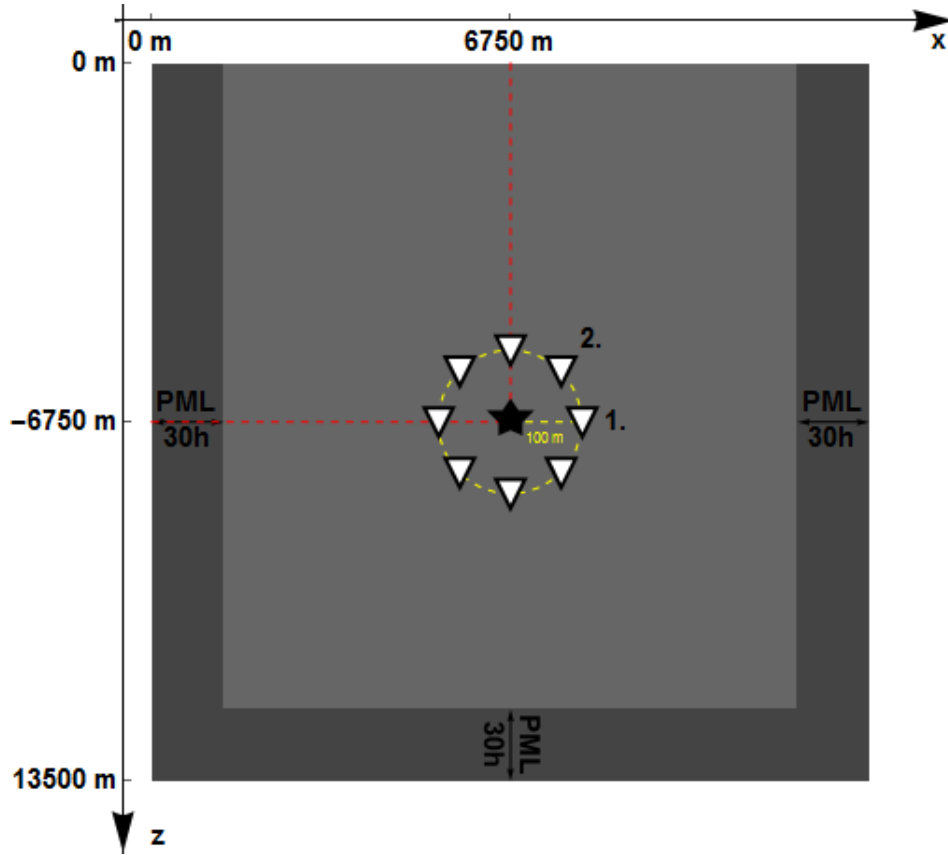


Figure 4 Source-receiver configuration.

The source-receiver configuration at Figure 4 is the same for each of the models with different size of the grid spacing. Receivers lie on the circle of the radius of 100 m that is centered at source location $[6750, -6750]$. The PML, with width of thirty times the grid spacing h , is applied at all boundaries except the top one, where free surface condition is satisfied.

The FD method for different grid spacing h was tested against an analytical solution for wave propagation in a porous medium. The analytical solution is given by Dai *et al.* (1995) for a homogenous porous medium with explosive dilatational line source. Material parameters, together with source parameters for numerical simulations in the Table 2 and 3 are the same as for analytical. The analytical solution used has $\eta = 0$, hence there is no damping included. Although $\eta = 0$ represents an inviscid fluid in a porous media, it allows us to verify the method against the exact analytical solution.

In order to reach better accuracy and to prevent the effect of interpolation of velocities from neighboring grid cells at the grid cell corresponding to specific receiver location, we could not fulfill the same source-receiver distance condition of 100 m for every proposed model. Therefore the abovementioned distance is different for different grid spacing, but very close to the value of 100 m . This not even provide better precision, but also preserve symmetry of receivers from opposite points around the circle that is centered at the source.

Corresponding analytical solutions are naturally also calculated with respect to source-receiver distance in numerical solution.

Numerical solutions for three different grid spacing and analytical solutions are compared in Figures 5–16. To clearly see all plotted waveforms, the analytical and numerical solutions have been normalized to one, using their maximum amplitude. Each figure contains horizontal and vertical components of solid phase velocity v_i and q_i velocity of fluid phase relative to that of solid phase for two different source-receiver positions. The position of receiver with respect to receiver is illustrated by little circle situated in q_x component plot.

As expected, the slow compressional wave is present at all components, since the viscosity is equal to zero and receivers are close to the source. From observation of synthetic seismograms, we can see that slow P-wave propagates with smaller speed than fast P-wave. This is in agreement with theoretical calculations of wave speeds. We also observe that the amplitude of the slow P-wave is stronger at q_i component, whereas its amplitude at v_i component is much weaker compared to the amplitude of fast P-wave.

Comparison of numerical and analytical solution for grid spacing $h = 5\text{ m}$ shows oscillatory tails present at this large grid spacing caused by numerical dispersion. However, for grid spacing $h = 3\text{ m}$ and $h = 1.5\text{ m}$, the visual inspection clearly shows that the numerical and analytical solutions match extremely well with no or very small visible difference.

In order to quantify the comparison between the analytical and numerical signals, we have used misfit criteria, following the work of Kristeková *et al.* (2006). The misfit criteria are based on the time-frequency representation of the seismograms obtained as the continuous wavelet transform with the analyzing Morlet wavelet. The misfit criteria include time-frequency envelope (TFEM) and phase misfits (TFPM), time-dependent envelope (TEM) and phase misfits (TPM), frequency-dependent envelope (FEM) and phase misfits (FPM), and single-valued envelope (EM) and phase misfits (PM). For brevity, we only calculated misfits for receiver one and two located at the positions, which are illustrated in Figure 4. The misfits for receiver one are depicted in Figures 17-19 and for two in Figure 20-22. Each of these figures contains TFEM, TFPM, TPM, FEM and FPM of v_x, v_z and q_x, q_z components.

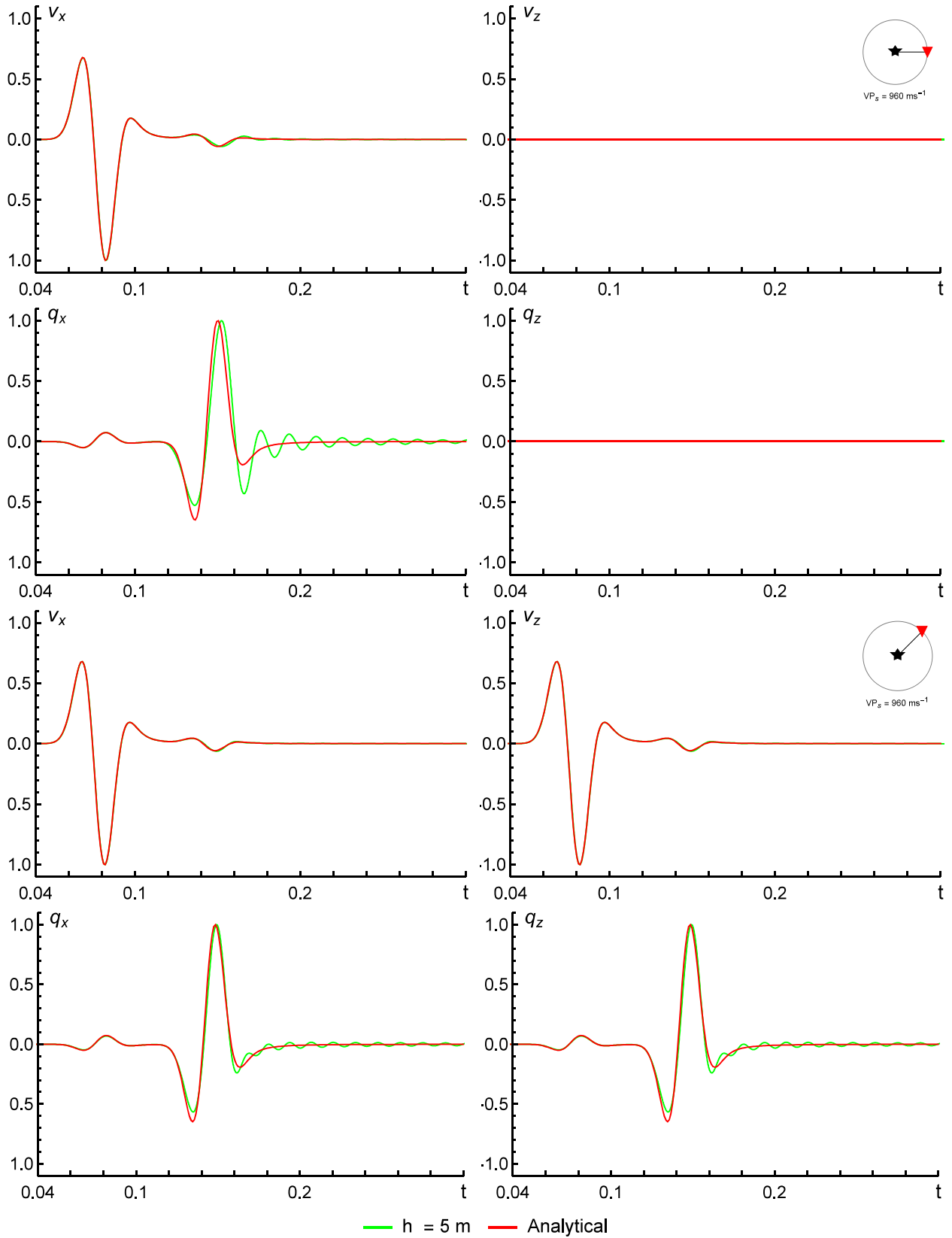


Figure 5. Comparison of our FD synthetics with analytical solutions. Red triangles indicate receiver positions. Black star indicates the line source. v_x , v_z and q_x , q_z indicate the x and z -components of the particle velocity in the solid phase, and x and z -components of the velocity of fluid phase relative to that of solid phase. $h = 5 \text{ m}$ indicates the size of the grid spacing in the FD simulation.

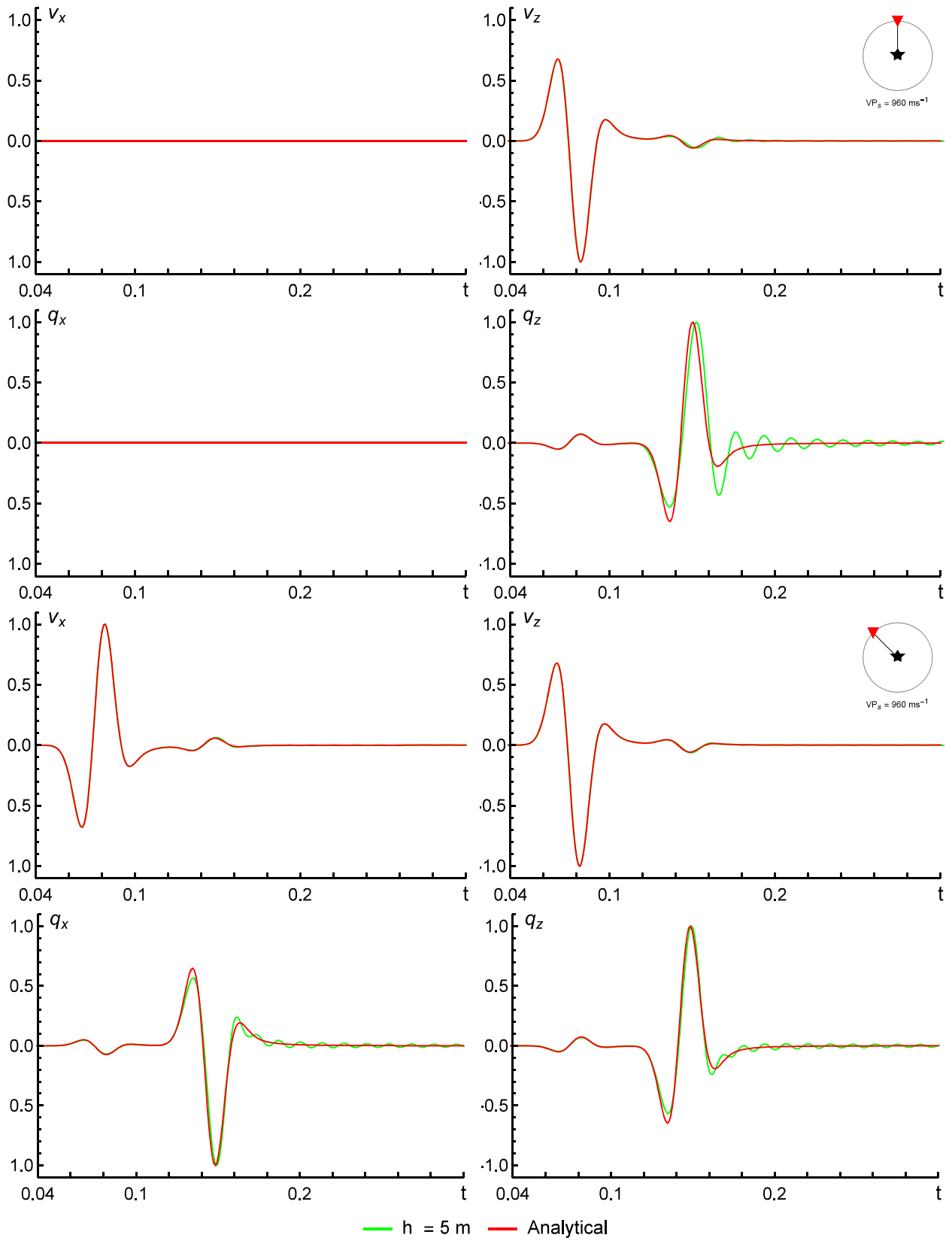


Figure 6. The same as in Fig. 5 but for the indicated receiver positions.

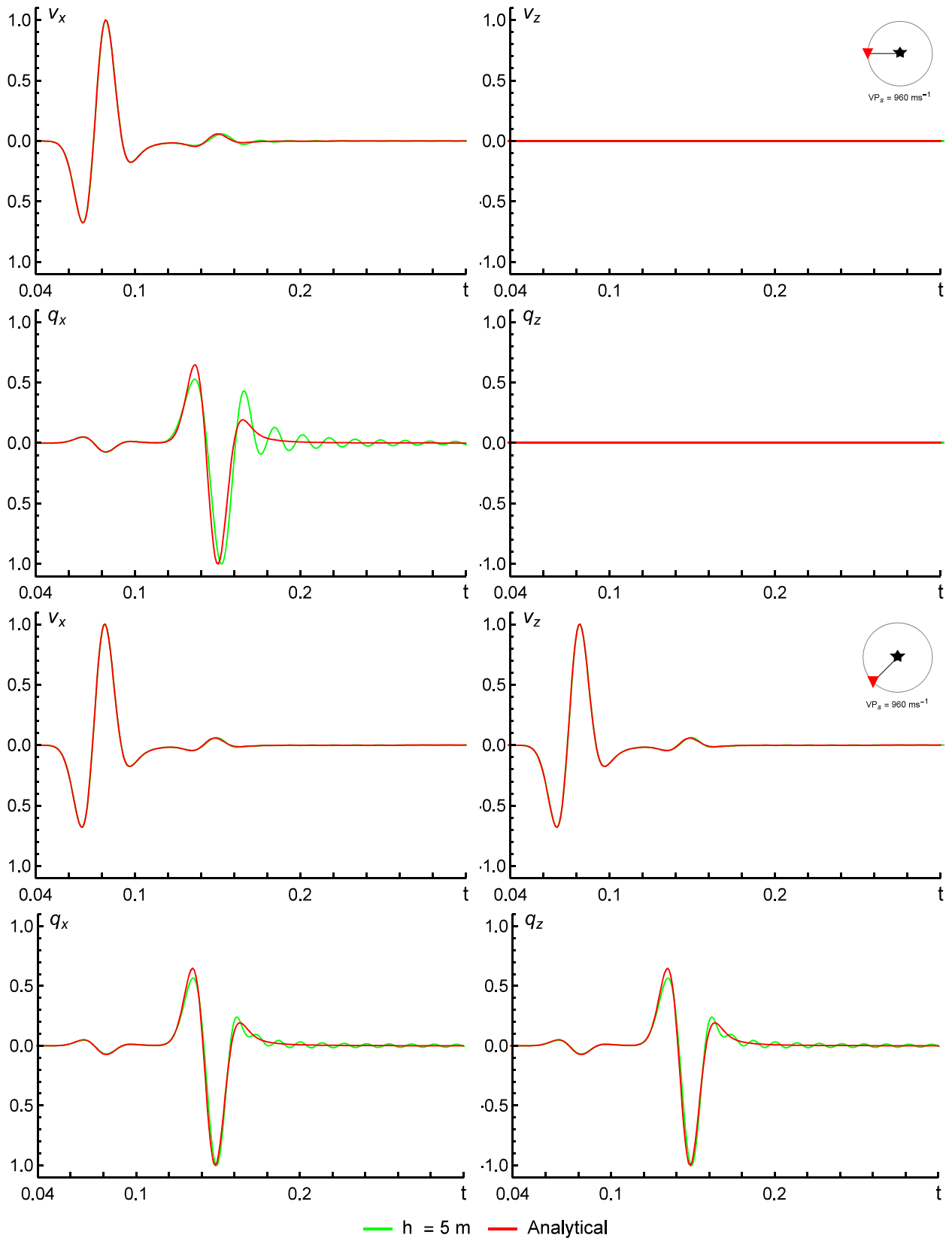


Figure 7. The same as in Fig. 5 but for the indicated receiver positions.

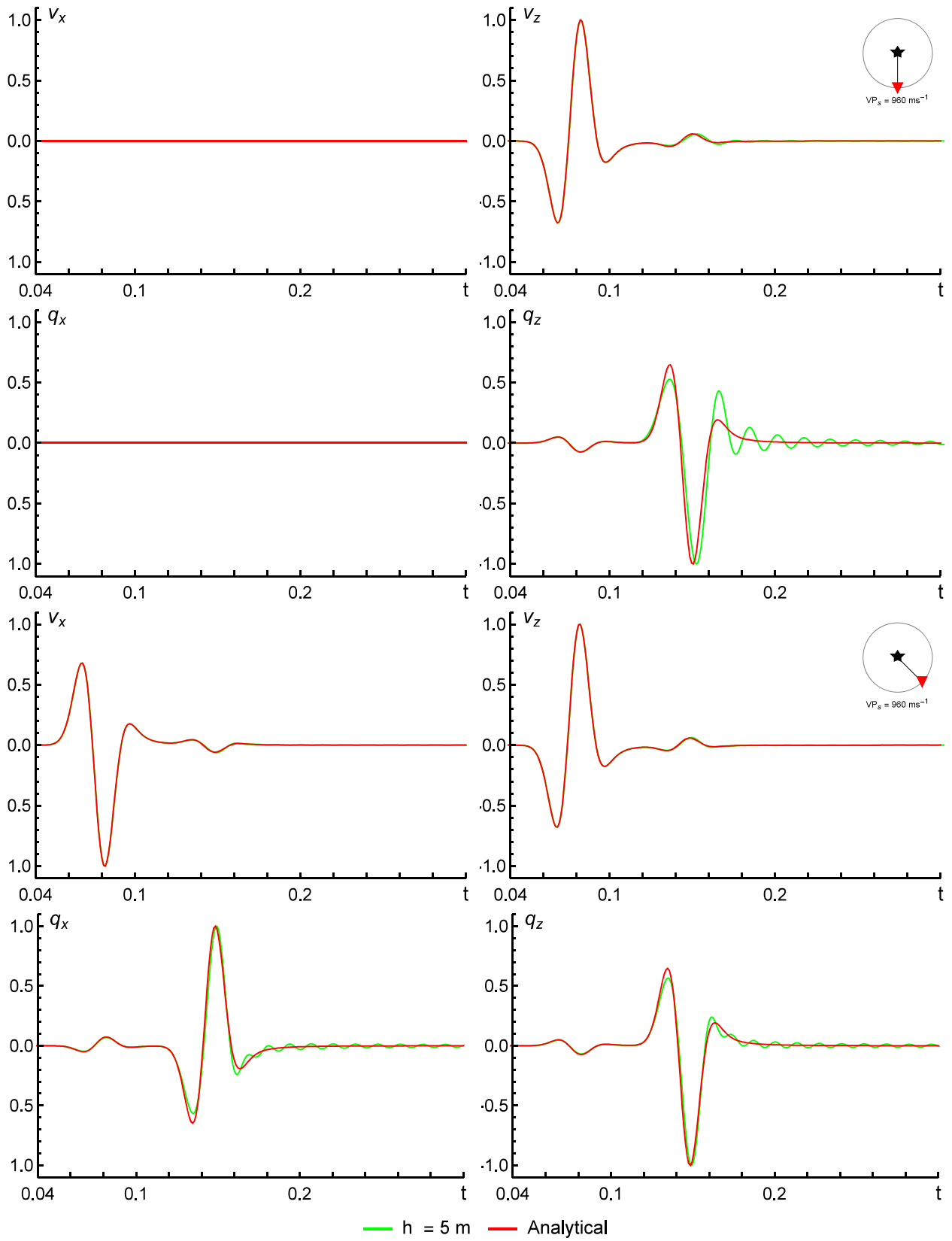


Figure 8. The same as in Fig. 5 but for the indicated receiver positions.

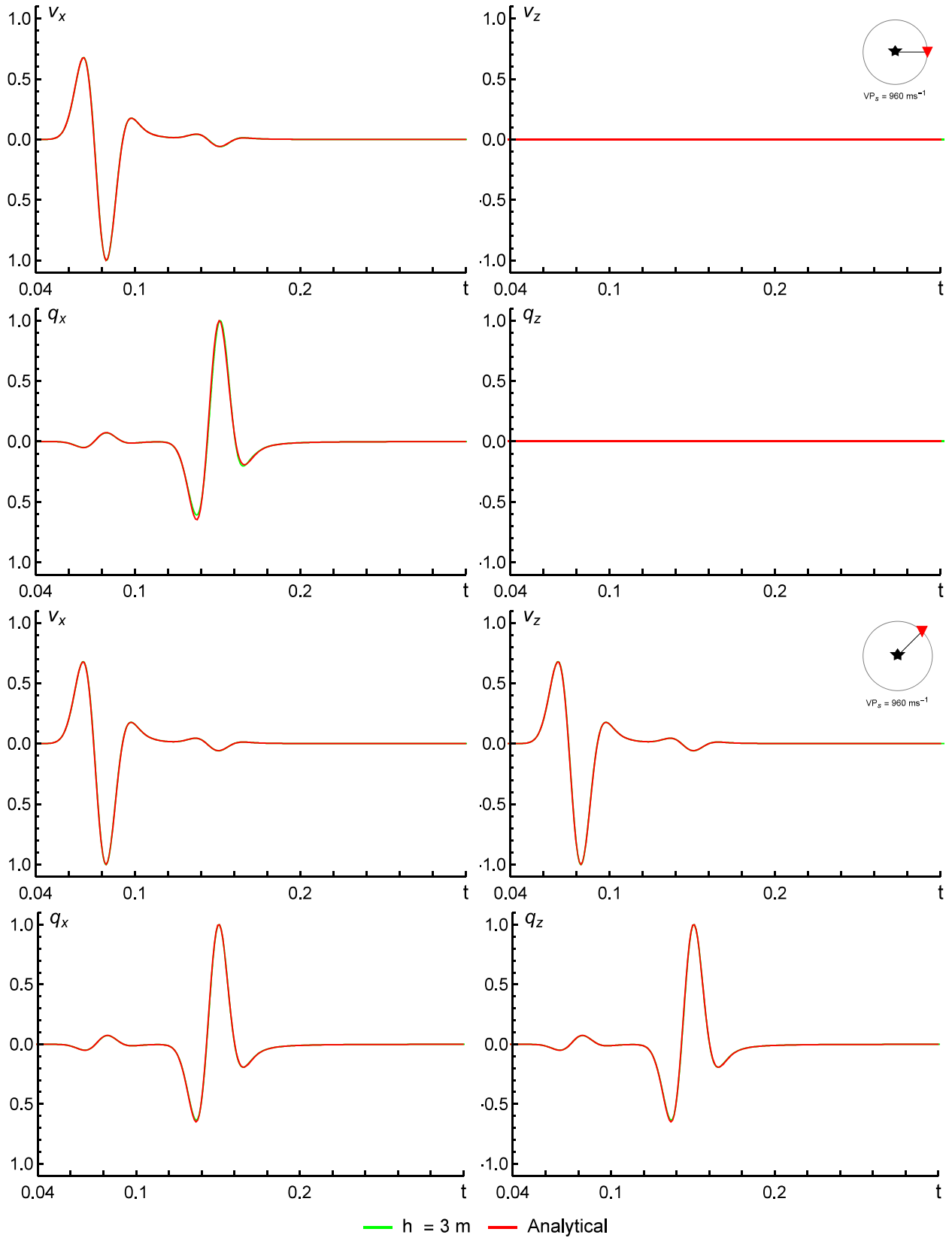


Figure 9. Comparison of our FD synthetics with analytical solutions. Red triangles indicate receiver positions. Black star indicates the line source. v_x, v_z and q_x, q_z indicate the x and z -components of the particle velocity in the solid phase, and x and z -components of the velocity of fluid phase relative to that of solid phase. $h = 3 \text{ m}$ indicates the size of the grid spacing in the FD simulation.

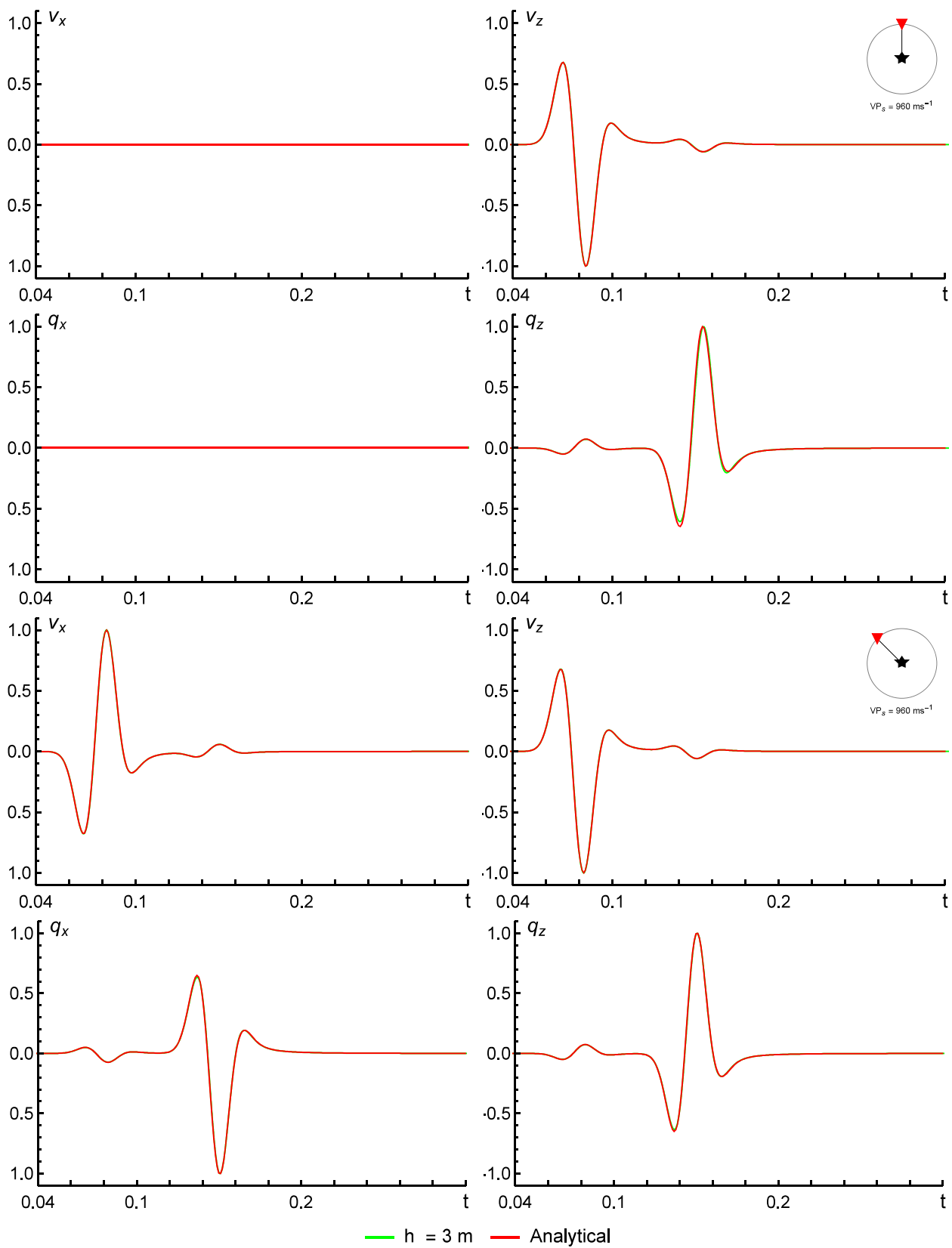


Figure 10. The same as in Fig. 9 but for the indicated receiver positions.

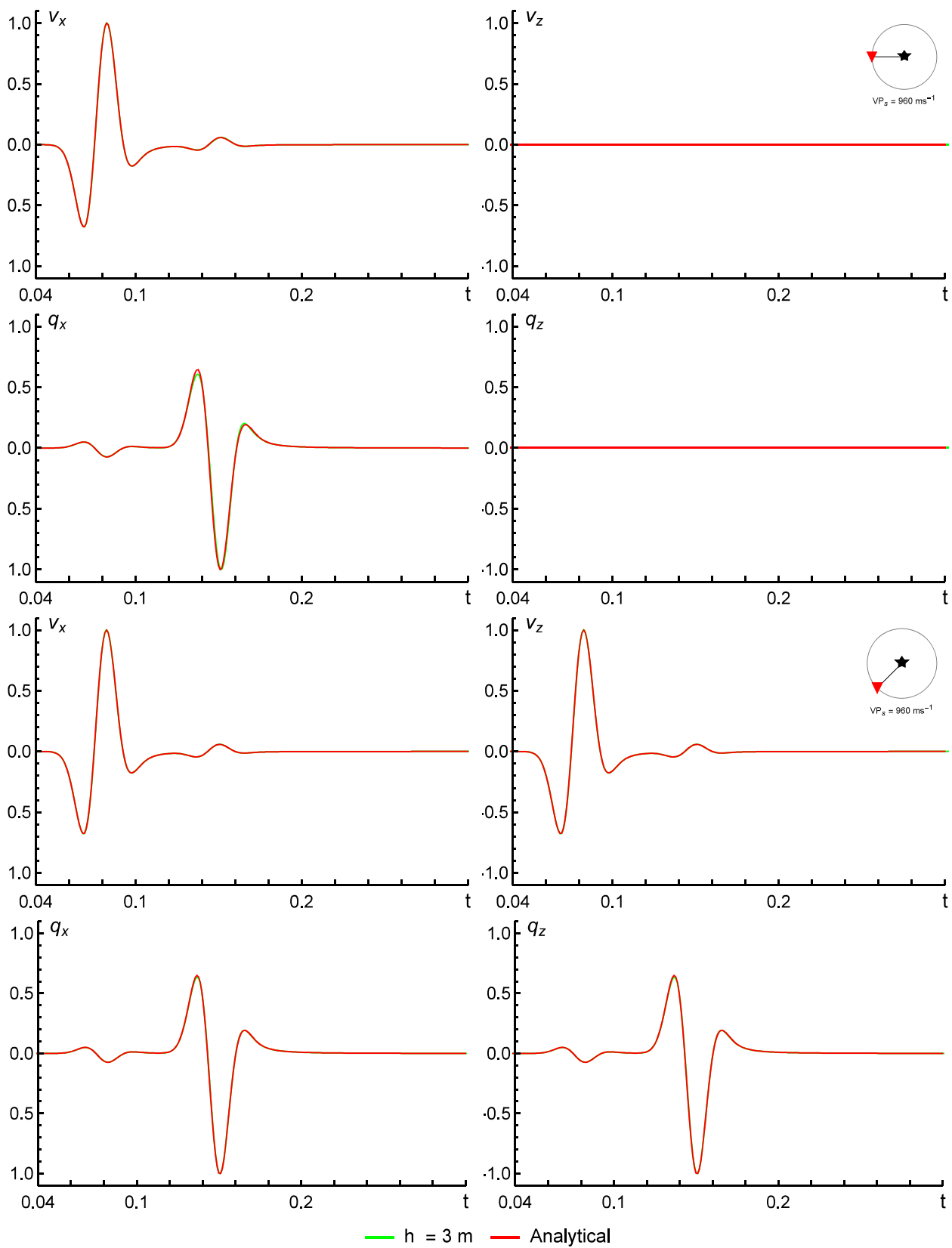


Figure 11. The same as in Fig. 9 but for the indicated receiver positions.

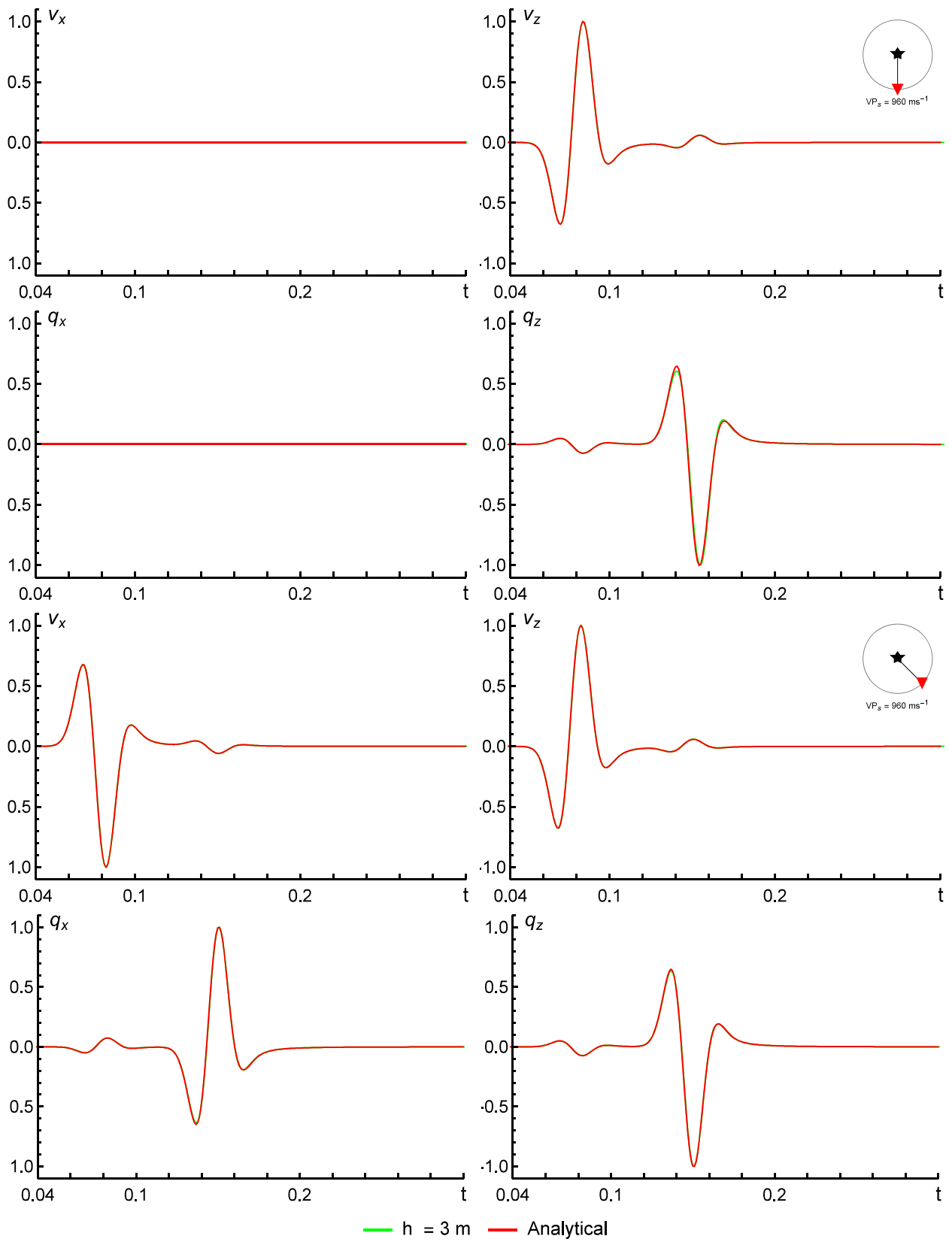


Figure 12. The same as in Fig. 9 but for the indicated receiver positions.

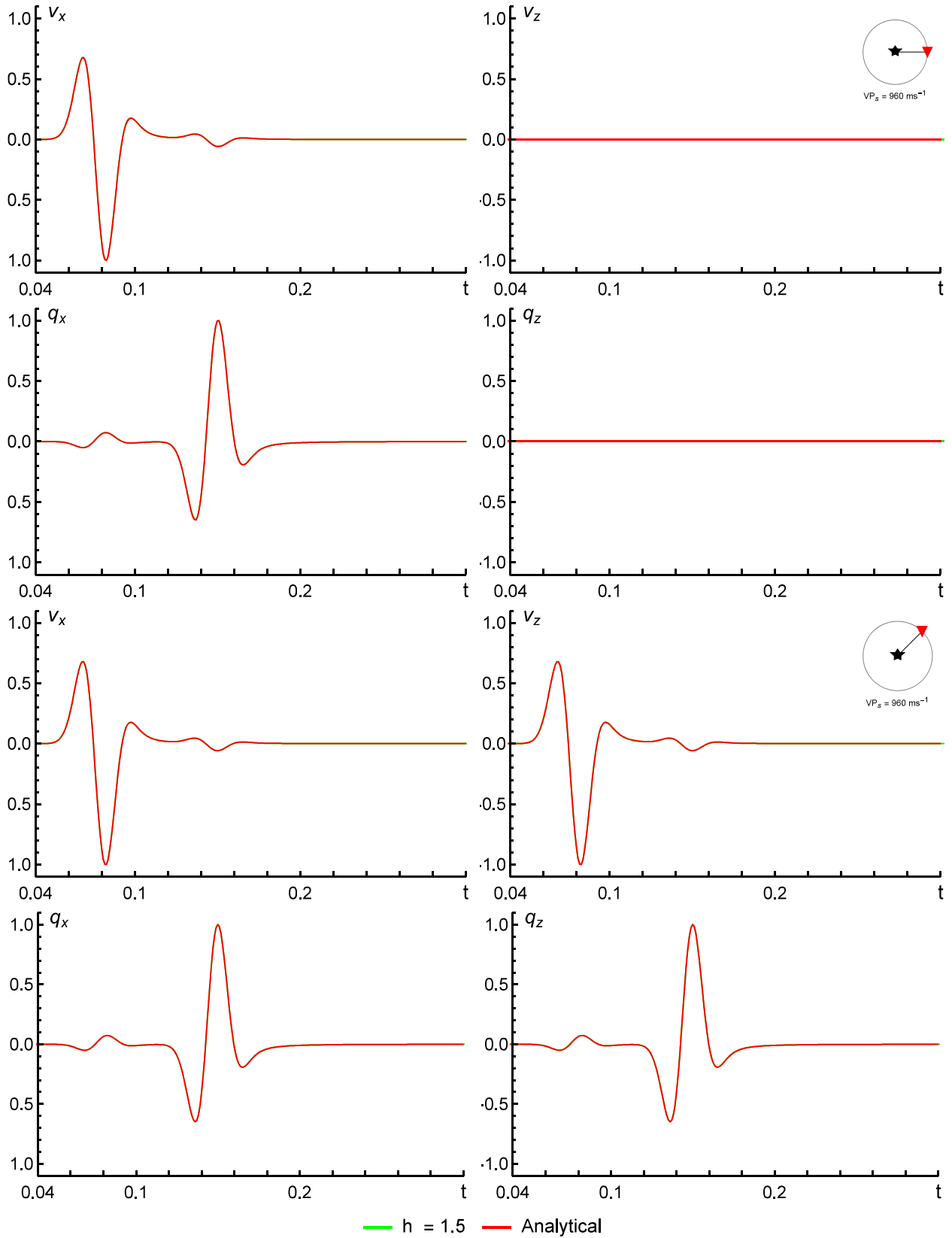


Figure 13. Comparison of our FD synthetics with analytical solutions. Red triangles indicate receiver positions. Black star indicates the line source. v_x, v_z and q_x, q_z indicate the x and z -components of the particle velocity in the solid phase, and x and z -components of the velocity of fluid phase relative to that of solid phase. $h = 1.5 \text{ m}$ indicates the size of the grid spacing in the FD simulation.

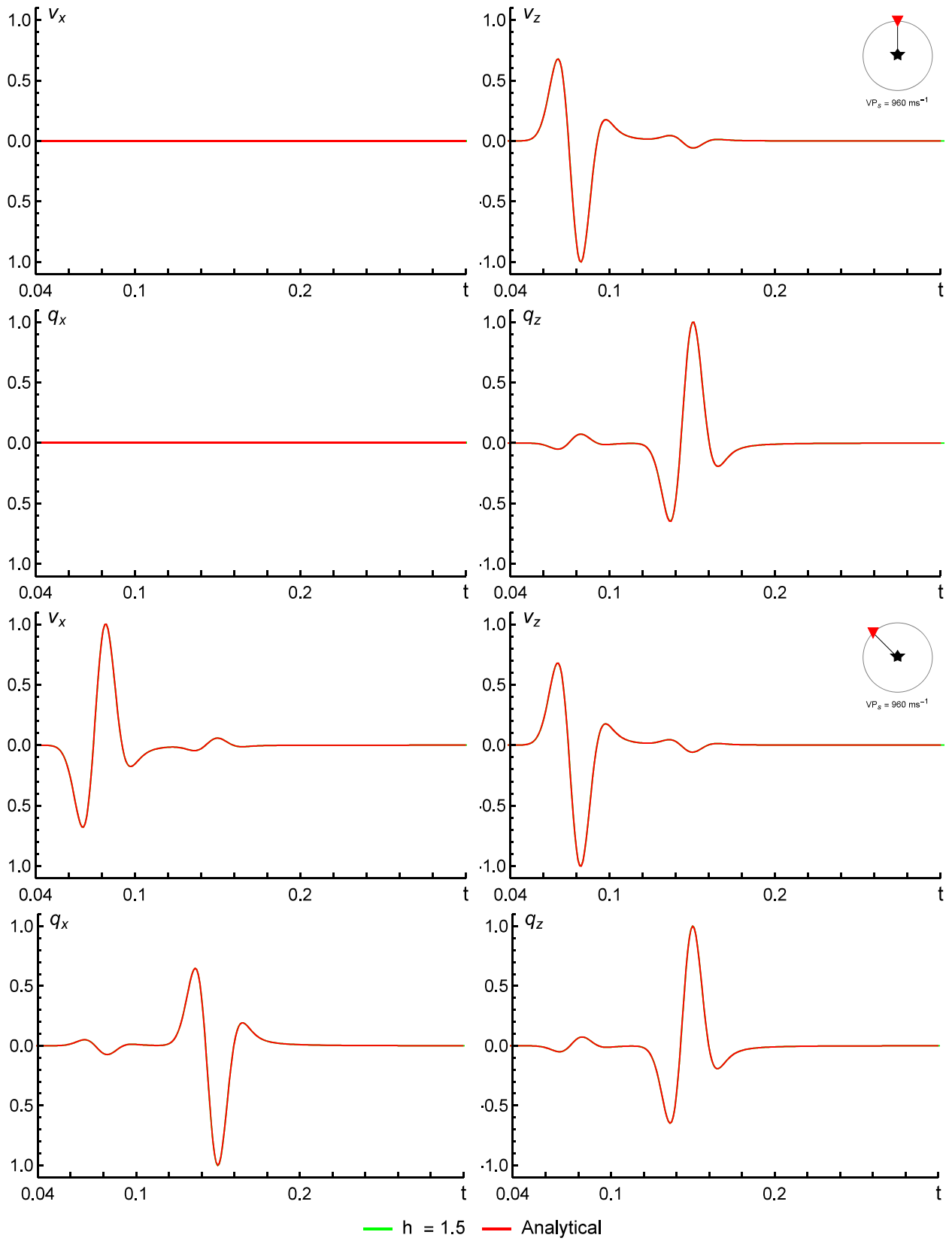


Figure 14. The same as in Fig. 13 but for the indicated receiver positions.

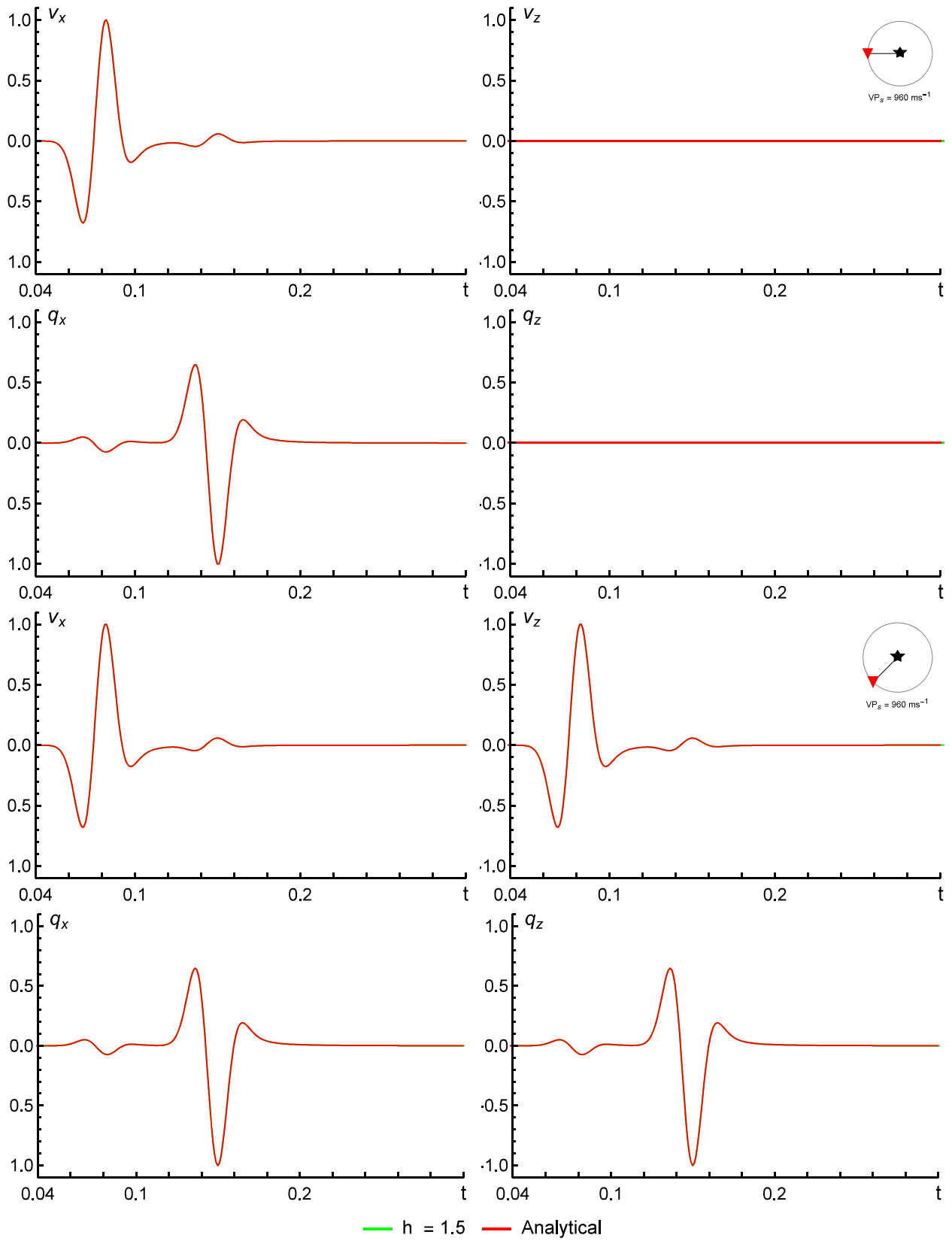


Figure 15. The same as in Fig. 13 but for the indicated receiver positions.

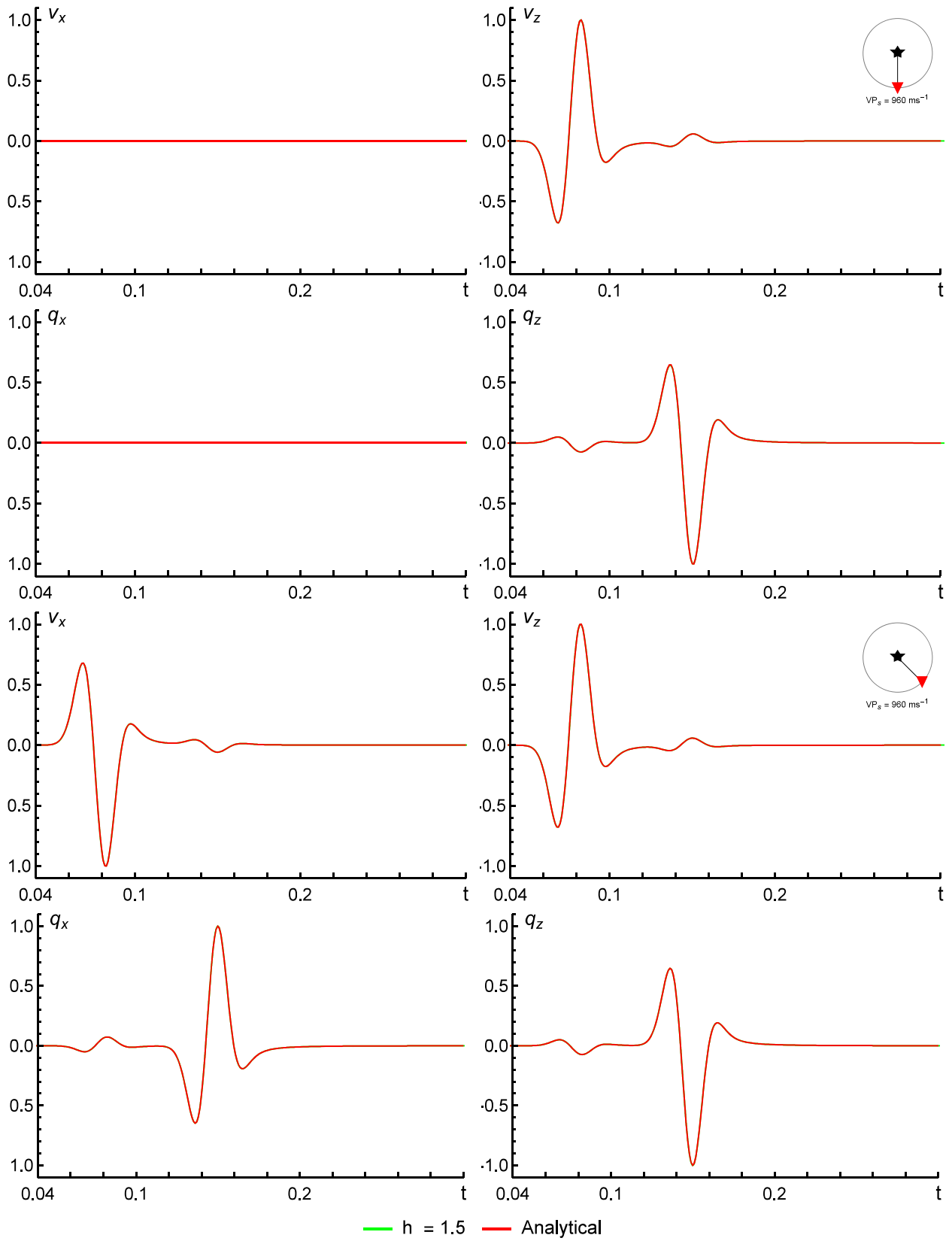


Figure 16. The same as in Fig. 13 but for the indicated receiver positions.

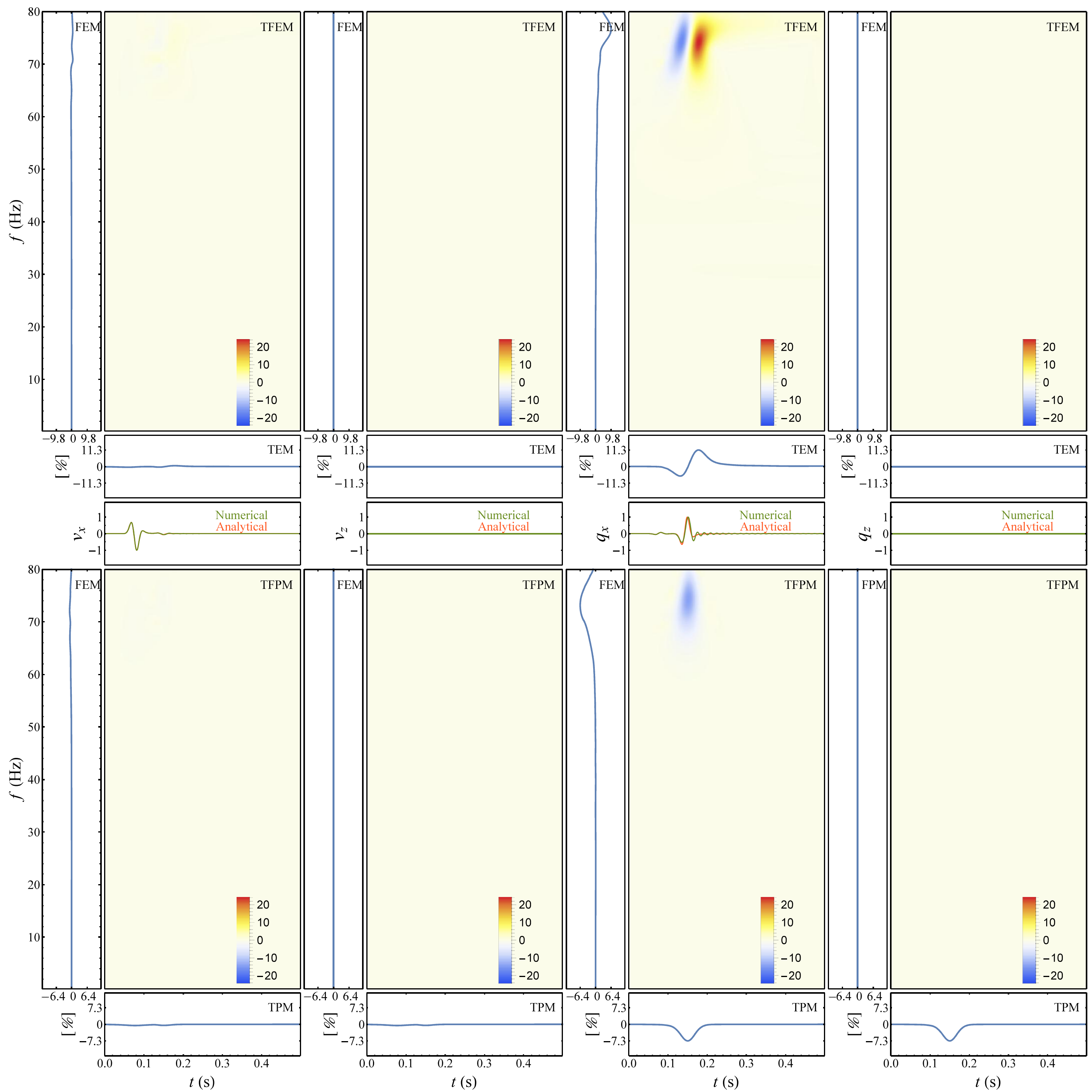


Figure 17. Envelope and phase misfits between the FD synthetics ($h = 5\text{ m}$) and analytical solutions for receiver 1.

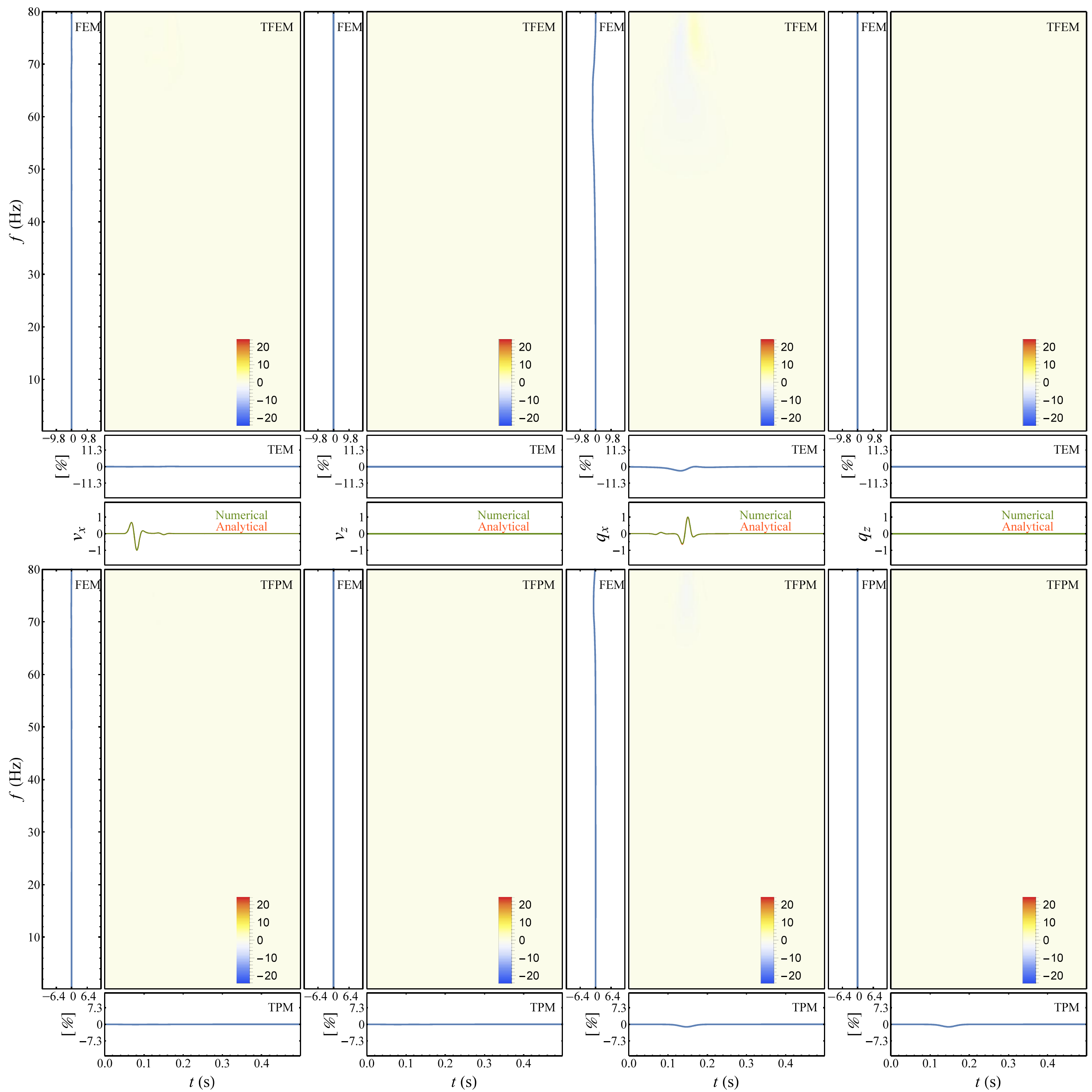


Figure 18. Envelope and phase misfits between the FD synthetics ($h = 3\text{ m}$) and analytical solutions for receiver 1.

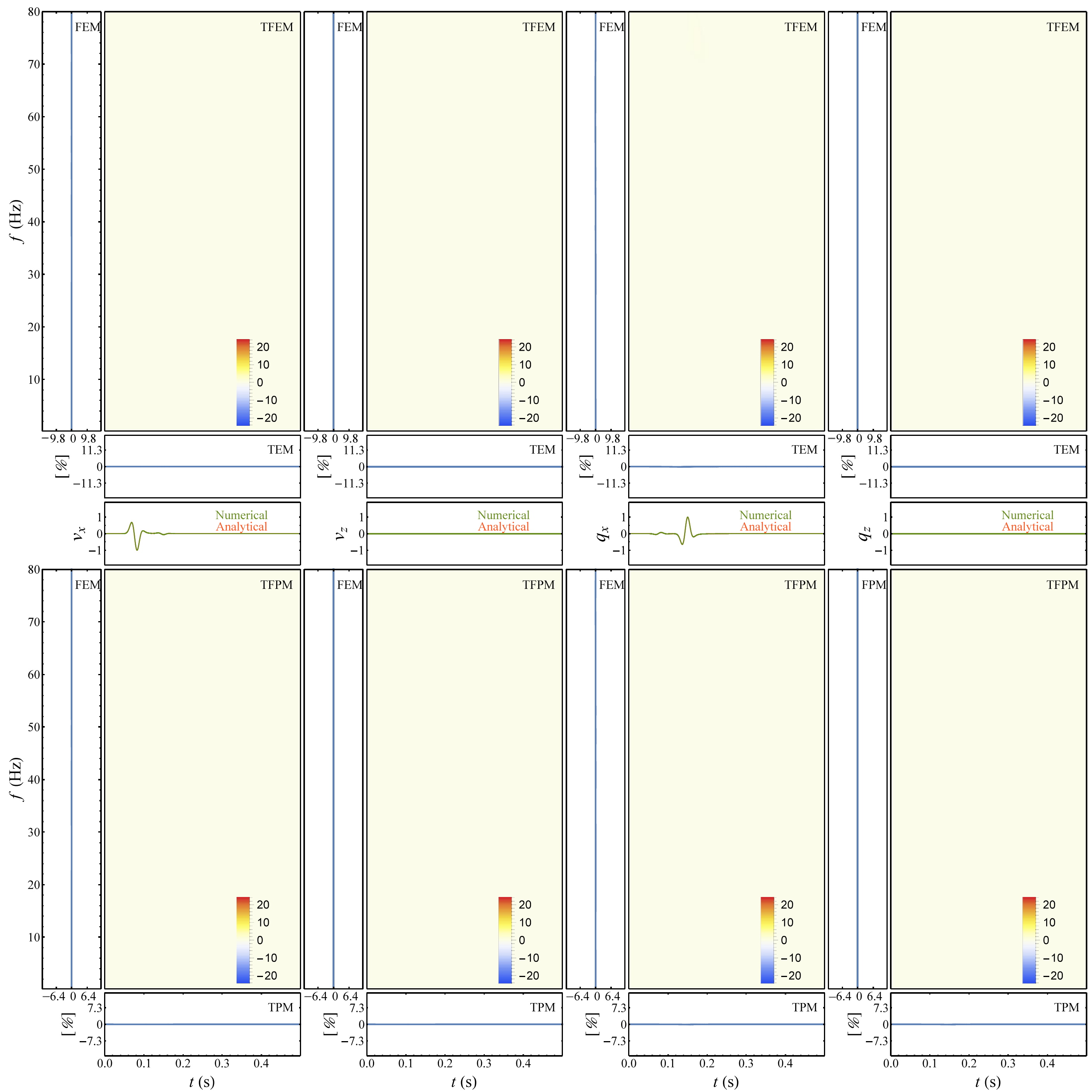


Figure 19. Envelope and phase misfits between the FD synthetics ($h = 1.5 \text{ m}$) and analytical solutions for receiver 1.

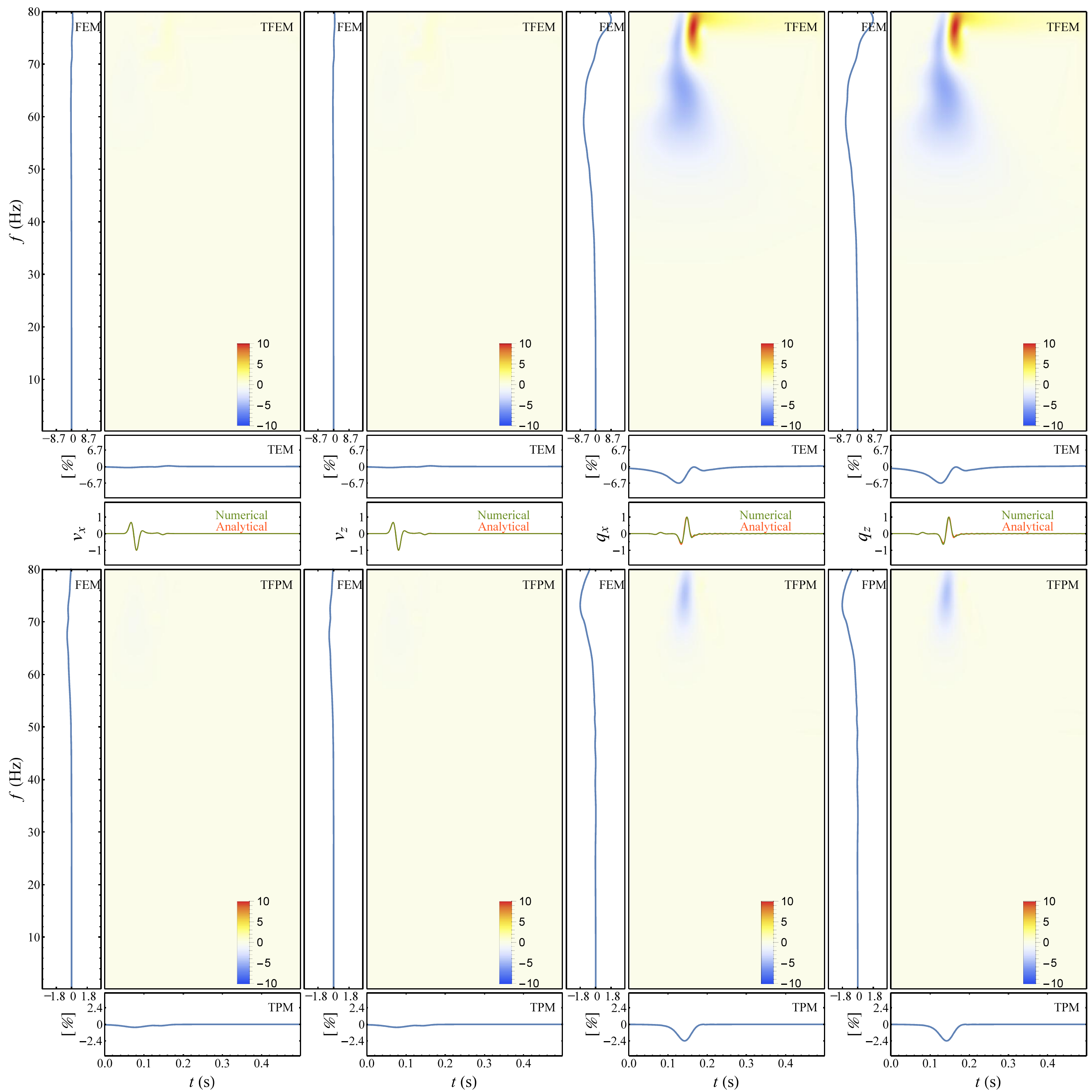


Figure 20. Envelope and phase misfits between the FD synthetics ($h = 5\text{ m}$) and analytical solutions for receiver 2.

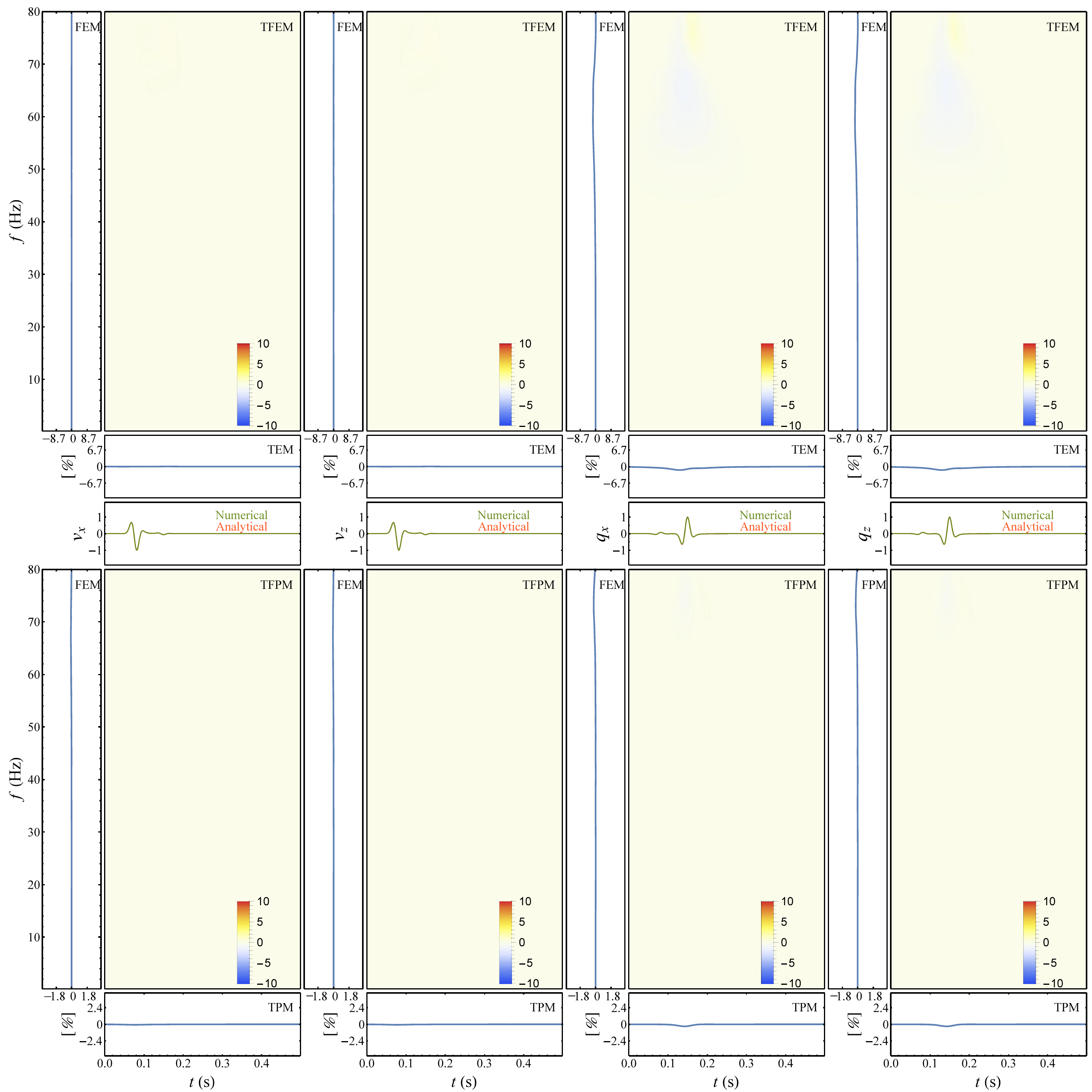


Figure 21. Envelope and phase misfits between the FD synthetics ($h = 3\text{ m}$) and analytical solutions for receiver 2.

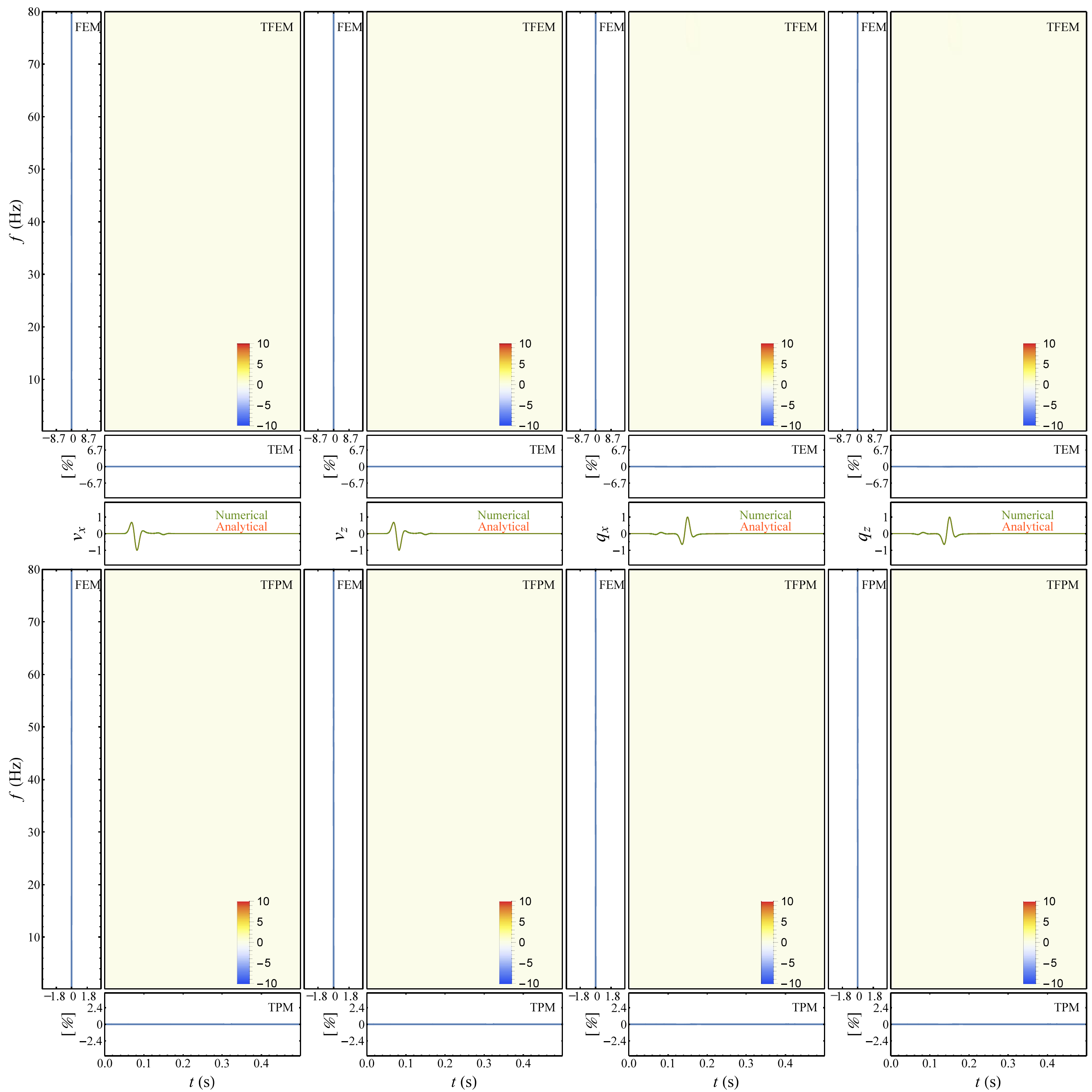


Figure 22. Envelope and phase misfits between the FD synthetics ($h = 1.5\text{ m}$) and analytical solutions for receiver 2.

The misfits for both the solid and fluid velocities in Figures 17-19 and Figures 20-22 show that the numerical methods give a very good fit with the analytical solution as grid spacing is decreasing.

As we can see, the TFEM, TFPM, TPM, FEM and FPM for 1. receiver take bigger values than for 2. receiver. This is due to the fact, that grid dispersion is strongest for wave propagating along a coordinate axis (1. receiver case) and weaker for a wave propagating along plane diagonal (2. receiver case). This was demonstrated by Moczo *et al.* (2000).

By comparison of misfits corresponding to solid velocity and misfits corresponding to velocity of fluid phase relative to that of solid phase, one can observe that values of different misfit functions are in general smaller for solid phase. This is specially visible in time-frequency envelope plot. We know that to avoid the effect of numerical grid dispersion, we have to sampled the minimal wavelength (in our case is the wavelength corresponding to slow P-wave) by certain number of samples. This was clearly violated for model with grid spacing $h = 5\text{ m}$ and therefore in this case fast wave with bigger wavelength fit analytical solution better than undersampled wavelength of slow wave. If we now restrict ourselves on part of seismograms where slow wave is present, and if we realize that the TFEM is more sensitive on bigger wave amplitudes, we come to the conclusion that even if the matching of analytical and numerical are the same in the region of slow wave presence for both the v_i and q_i component, the amplitude difference between mentioned components affect the TFEM the most.

In order to verify the spatial convergence of our scheme, we have also computed single-valued envelope (EM) and single-valued phase (PM) misfits for every model. For brevity, we only show here single-valued misfits for 1. receiver in Figure 23. As we can see, the single-valued misfits fit 4th-order curve (denoted by purple line) very well.

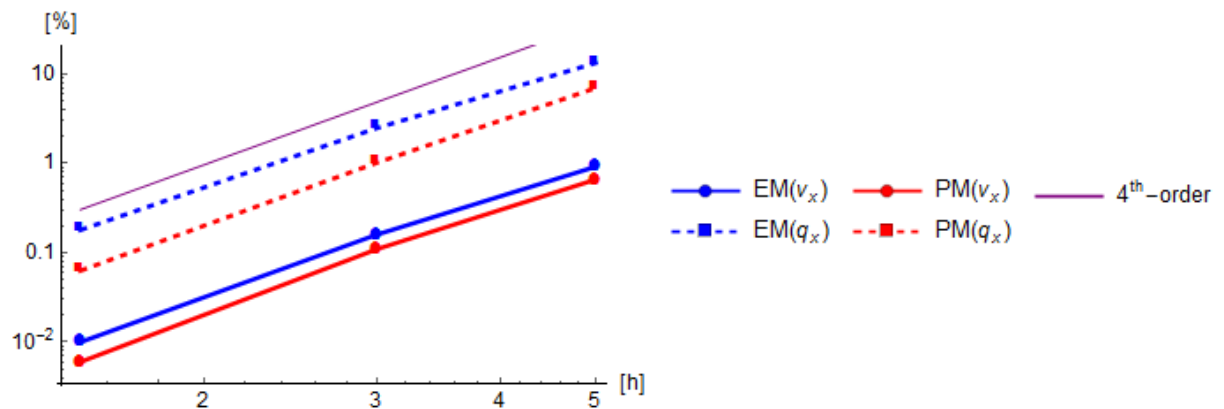


Figure 23. Single-valued envelope and single-valued phase misfits for receiver 1.

6 Conclusions

In this master's thesis we have:

- presented an overview of equations of poroelasticity relevant for seismic wave propagation in poroelastic medium
- developed a numerical scheme using two-dimensional, staggered, 2nd-order accurate in time and 4th-order accurate in space, finite-difference method on a uniform rectangular grid
- developed a computational algorithm for simulating wave propagation in the poroelastic medium
- encoded computational algorithm in a FORTRAN 95 program
- implemented AFDA for simulating a planar free surface, PML for simulating absorbing boundaries, excitation of wavefield by line source
- numerically tested the developed algorithm and computer code for model of an unbounded homogeneous poroelastic medium
- demonstrated an optional level of agreement of our numerical solution with an analytical solution

The developed algorithm provides a basis for further methodological development. That will be aimed in incorporation realistic attenuation in the computational model.

References

- Biot, M.A. 1956. Theory of propagation of elastic waves in a fluid saturated porous solid, I. Low-frequency range. *J. acoust. Soc. Am.* 28, 168-178.
- Boutin, C., G. Bonnet, P. Y. Bard 1986. Green functions and associated sources in infinite and stratified poroelastic media. *Journal of Geophysical Research* 90, 521-550.
- Burridge, R., C. A. Vargas 1978. The fundamental solution in dynamic poroelasticity. *Journal of Geophysical Research* 58, 61-90.
- Carcione, J. M. 1996a. Wave propagation in anisotropic, saturated porous media: Plane-wave theory and numerical simulation. *J. acoust. Soc. Am.* 99, 2655–2666.
- Carcione, J. M. 1996b. Full frequency-range transient solution for P-waves in a fluid-saturated viscoacoustic porous medium. *Geophysical prospecting* 44, 99-129.
- Carcione, J. M., H. B. Helle, N. H. Pham 2003. White's model for wave propagation in partially saturated rocks: Comparison with poroelastic numerical experiments. *Geophysics* 68, 1389–1398.
- Carcione, J. M., Ch. Morency, J. E. Santos 2010. Computational poroelasticity - A review. *Geophysics* 75, 229-243.
- Carcione, J. M. 2014. Wave Fields in Real Media: Wave Propagation in Anisotropic, Anelastic, Porous and Electromagnetic Media. Amsterdam: Elsevier.
- Dai, N., A. Vafidis, E. Kanasevich 1995. Wave propagation in heterogeneous porous media: A velocity-stress, finite-difference method. *Geophysics* 60, 327–340.
- de la Cruz, V., T. J. Spanos 1985. Seismic wave propagation in a porous medium. *Geophysics* 50, 1556-1565.
- de la Puente, J. 2008a. Seismic wave propagation for complex rheologies. VDM Verlag Dr. Muller, Saarbrücken.
- de la Puente, J., M. Dumbser, M. Käser, H. Igel 2008b. Discontinuous Galerkin methods for wave propagation in poroelastic media. *Geophysics* 73, T77-T97.
- Dutta, N.C., H. Ode 1979a. Attenuation and dispersion of compressional waves in fluid-filled porous rocks with partial gas saturation (White model)—part I: Biot theory. *Geophysics* 44, 1777–1788.
- Dutta, N.C., H. Ode 1979b. Attenuation and dispersion of compressional waves in fluid-filled porous rocks with partial gas saturation (White model)—part II: results. *Geophysics* 44, 1789–1805.
- Dutta, N.C., A. J. Seriff 1979. On White's model of attenuation in rocks with partial saturation. *Geophysics* 44, 1806–1812.

- Gurevich, B., A. P. Sadovnichaja, S. L. Lopatnikov, and S. A. Shapiro 1998. Scattering of a compressional wave in a poroelastic medium by an ellipsoidal inclusion. *Geophysical Journal International* 133, 91–103.
- Gregor, D. 2014. Physics of seismic wave propagation in poroelastic media. Bachelor thesis. Bratislava.
- Hsieh, M., L. Zhao, K. Ma 2011. Realistic Earthquake Ground Motion Prediction by Physics-Based Numerical Simulations. *Am. Geophysical Union 2011*.
- Komatitsch, D., R. Martin 2007. An unsplit convolutional perfectly matched layer improved at grazing incidence for the seismic wave equation. *Geophysics* 72, SM155–SM167.
- Kristek, J., P. Moczo, R. J. Archuleta 2002. Efficient methods to simulate planar free surface in the 3D 4th-order staggered-grid finite-difference schemes. *Studia Geophys. Geod.* 46, 355–381.
- Kristek, J., P. Moczo, M. Gális 2009. A brief summary of some PML formulations and discretizations for the velocity-stress equation of seismic motion. *Studia Geophys. Geod.* 53, 459–474.
- Kristek, J., P. Moczo, M. Gális 2010. Stable discontinuous staggered grid in the finite-difference modelling of seismic motion. *Geophys. J. Int.* 183, 1401–1407.
- Kristek, J., P. Moczo 2003. Seismic wave propagation in viscoelastic media with material discontinuities – a 3D 4th-order staggered-grid finite-difference modeling. *Bull. Seism. Soc. Am.* 93, 2273–2280.
- Kristekova, M., J. Kristek, P. Moczo, S. M. Day 2006. Misfit criteria for quantitative comparison of seismograms. *Bull. Seism. Soc. Am.* 96, 1836–1850.
- Lay, T., T. C. Wallace 1995. Modern Global Seismology. Academic Press. USA.
- Levander, A. R. 1988. Fourth-order finite-difference P-SV seismograms. *Geophysics* 53, 1425–1436.
- Moczo, P., J. Kristek 2005. On the rheological models used for time-domain methods of seismic wave propagation. *Geophys. Res. Lett.* 32, L01306.
- Moczo, P., J. Kristek, M. Gális 2004. Simulation of planar free surface with near-surface lateral discontinuities in the finite-difference modeling of seismic motion. *Bull. Seism. Soc. Am.* 94, 760–768.
- Moczo, P., J. Kristek, M. Gális 2014. The Finite-Difference Modelling of Earthquake Motions. *Cambridge University Press*.
- Moczo, P., J. Kristek, M. Gális, E. Chaljub, V. Etienne 2011. 3D finite-difference, finite-element, discontinuous-Galerkin and spectral-element schemes analysed for their accuracy with respect to P-wave to S-wave speed ratio. *Geophys. J. Int.* 187, 1645–1667.

- Moczo, P., J. Kristek, M. Gális, P. Pažák, M. Balažovjeh 2007a. The finite-difference and finite-element modeling of seismic wave propagation and earthquake motion. *Acta Physica Slovaca* 47, 177-406.
- Moczo, P., J. Kristek, L. Halada 2000. 3D fourth-order staggered-grid finite-difference schemes: stability and grid dispersion. *Bull. Seism. Soc. Am.* 90, 587-603.
- Moczo, P., J. Kristek, V. Vavrycuk, R. J. Archuleta, L. Halada 2002. 3D heterogeneous staggered-grid finite-difference modeling of seismic motion with volume harmonic and arithmetic averaging of elastic moduli and densities. *Bull. Seism. Soc. Am.* 92, 3042-3066.
- Morency, Ch., J. Tromp 2008. Spectral-element simulations of wave propagation in porous media. *Geophys. J. Int.* 175, 301-345.
- O'Brien, G. S. 2010. 3D rotated and standard staggered finite-difference solutions to Biot's poroelastic wave equations: Stability condition and dispersion analysis. *Geophysics* 75, T111-T119.
- Özdenvar, T., G. A. McMechan 1997. Algorithms for staggered-grid computations for poroelastic, elastic, acoustic, and scalar wave equations. *Geophysical Prospecting* 45, 403-420.
- Pride, S.R., E. Tromeur, J. G. Berryman 2002. Biot slow-wave effects in stratified rock. *Geophysical Journal International* 67, 271-281.
- Roberts, A. P., E. J. Garboczi 2002. Computation of the linear elastic properties of random porous materials with a wide variety of microstructure. *Proceedings of the Royal Society of London* 458, 1033-1054.
- Shapiro, S.A., T. M. Müller 1999. Seismic signatures of permeability in heterogeneous porous media. *Geophysics* 64, 99-103.
- Sheen, D., K. Tuncay, C. Baag, P. Ortoleva 2006. Parallel implementation of a velocity-stress staggered-grid finite-difference method for 2-D poroelastic wave propagation. *Computers & Geosciences* 32, 1182-1191.
- Wang, H. F. 2000. Theory of Linear Poroelasticity with Applications to Geomechanics and Hydrogeology. Princeton University Press, Princeton, New Jersey.
- White, J. E. 1975. Computed Seismic speeds and attenuation in rocks with partial gas saturation. *Geophysics* 40, 224-232.
- White, J.E., N. G. Mikhaylova, F.M. Lyakhovitskiy 1975. Low-frequency seismic waves in fluid saturated layered rocks. *Izvestija Acad. Sci. USSR, Phys. Solid Earth* 11, 654-659.
- Wu, R., K. Aki 1989. Scattering and Attenuation of Seismic Waves. Berlin: Springer.

- Zeng, Q. Z., Q. H. Liu 2001. A staggered-grid finite-difference method with perfectly matched layers for poroelastic wave equations. *Journal of the Acoustical Society of America* 109, 2571-2580.
- Zhang, J. 1999. Quadrangle-grid velocity-stress finite difference method for poroelastic wave equations. *Geophysical Journal International* 139, 171–182
- Zhu, X., G. A. McMechan 1991. Numerical simulation of seismic responses of poroelastic reservoirs using Biot theory. *Geophysics* 56, 328-339.

Abstract

Numerical simulations have been more widely used in recent years as the speed of computers has increased. Such computer simulations have been proven to be particularly useful in relation of ground motion modeling in and around sedimentary basins from large earthquake. The approach of numerical modelling has been motivated by need of earthquake ground motion prediction at locations with no or insufficient earthquake recordings. The distribution and strength of ground motion can be affected by many geophysical and geological factors. For example, complex local structure not only changes the arrival times and amplitudes of individual seismic phases, it can also drastically alter local amplitude of surface ground motion. For more realistic ground motion prediction at local water-saturated sedimentary structures we need to incorporate poroelasticity in our computational model. Contrary to single-phase continuum (viscoelastic or viscoplastoelastic) it is necessary to consider presence of fluid-filled pores in media. In this master's thesis we have developed computational algorithm and computational code for numerical modelling of seismic wave propagation in a poroelastic medium based on the finite-difference method. We have verified the proper implementation of equations of poroelasticity in framework of the finite-difference method using extensive numerical tests and comparisons of the finite-difference simulations with exact solutions in the homogeneous unbounded poroelastic medium.

Key words: poroelastic media, wave propagation, seismic motion, finite-difference method

Zusammenfassung

Mit der zunehmenden Geschwindigkeit der Computer wurden numerische Simulationen in den letzten Jahren immer weiter verbreitet. Solche Computersimulationen haben sich besonders im Zusammenhang mit der Bodenbewegungsmodellierung nach großen Erdbeben in und um Sedimentbecken als nützlich erwiesen. Der Ansatz der numerischen Modellierung wurde motiviert durch die Notwendigkeit der Vorhersage der Erdbebenbodenbewegung an Standorten mit keinen oder nur unzureichenden Erdbebenaufnahmen. Die Verteilung und Stärke der Bodenbewegung kann durch viele geophysikalische und geologische Faktoren beeinflusst werden. Komplexe lokale Struktur, zum Beispiel, verändert nicht nur die Ankunftszeiten und die Amplituden der einzelnen seismischen Phasen; es kann auch die lokale Amplitude der Oberflächenbewegung drastisch verändern. Für eine realistischere Bodenbewegungsvorhersage auf lokalen wassergesättigten Sedimentstrukturen müssen wir die Poroelastizität in unser Berechnungsmodell integrieren. Im Gegensatz zum (viskoelastischen oder viskoplastoelastischen) Ein-Phasen-Kontinuum ist es notwendig, das Vorhandensein von flüssigkeitsgefüllten Poren in den Medien in Betracht zu ziehen. In dieser Masterarbeit haben wir Computeralgorithmen und -codes zur numerischen Modellierung seismischer Wellenausbreitung in einem poroelastischen Medium erstellt, auf der Grundlage der Finite-Differenzen-Methode. Wir haben dabei die ordnungsgemäße Umsetzung der Gleichungen der Poroelastizität im Rahmen der Finite-Differenzen-Methode überprüft, mit umfangreichen numerischen Tests und Vergleichen der Finite-Differenzen-Simulationen mit den exakten Lösungen im homogenen unbegrenzten poroelastischen Medium.

Schlüsselwörter: poroelastische Medien, Wellenausbreitung, seismische Bewegungen, Finite-Differenzen-Methode

Dávid Gregor

Curriculum Vitae

Personal data

Name Dávid Gregor
Born 26.12.1991 in Bratislava, Slovakia
Nationality Slovak
E-mail gregor28@uniba.sk

Education

Since 2015 **Master student of Joint master study programme Physics of the Earth**, *Universität Wien*, Wien; Comenius University -The Faculty of Mathematics, Physics and Informatics, Bratislava.
2014–2015 **Master student of master study programme Physics of the Earth**, *Comenius University -The Faculty of Mathematics, Physics and Informatics*, Bratislava.
2011–2014 **B.Sc. in Physics**, *The Faculty of Mathematics, Physics and Informatics*, Bratislava.

Bachelor Thesis

Title *Physics of seismic wave propagation in poroelastic media*
Supervisors Professor Peter Moczo

Computer Skills

Programming languages Fortran, Mathematica, Matlab and C++
Operating systems Windows and Linux
Geophysical Software Seismic Unix